5

Cuprous Oxide (Cu_2O): A Unique System Hosting Various Excitonic Matter and Exhibiting Large Third-Order Nonlinear Optical Responses

Joon I. Jang
Department of Physics, Applied Physics and Astronomy, State University of New York at Binghamton
USA

1. Introduction

Owing to its unique crystal and coupled electronic structures, a dipole-forbidden direct-gap semiconductor cuprous oxide (Cu_2O) has gained considerable attention for studying fundamental exciton physics and relevant coherent phenomena, ultimately aiming at excitonic Bose-Einstein condensation (BEC) [Wolfe *et al.* (1995)]. Despite tremendous experimental efforts, however, excitons in Cu_2O undergo mysterious collisional loss at high densities, resulting in a loss rate given by $\tau_A^{-1} = An$, where A is an empirical coefficient for collisional Auger-type loss and n is the exciton gas density [Hulin *et al.* (1980); O'Hara *et al.* (1999a;b); O'Hara & Wolfe (2000)]. Detailed analysis based on time- and space-resolved photoluminescence (PL) studies suggested formation of *optically inactive* excitonic molecules (biexcitons) [Jang & Wolfe (2005; 2006a;c)]. The existence of such "dark matter" seems to explain the long-standing difficulties in achieving BEC of excitons in Cu_2O, which severely limits the experimental gas density far below the critical BEC density ($n_c \simeq 10^{17}$ cm^{-3} at 2 K) and the goal remains still elusive.

An exciton polariton (hereafter polariton) has emerged as a new candidate and condensation of polaritons in two-dimensional (2D) quantum-well microcavity structures was recently reported where multilayer Bragg mirrors confined the optical components [Balili *et al.* (2007); Christopoulos *et al.* (2007); Deng *et al.* (2003; 2010); Kasprzak *et al.* (2006); Lagoudakis *et al.* (2008); Lai *et al.* (2007); Utsunomiya *et al.* (2008)]. Even under strong cavity confinement, however, this "nonequilibrium" polariton BEC lasts only for several picoseconds, basically due to the short-lived excitonic component undergoing efficient dipole transitions in host semiconducting materials. The polariton lifetimes of this time scale is difficult to utilize for future optoelectronic applications.

Quadrupole polaritons in Cu_2O may offer an alternative route to "long-lived" BEC. Unlike well-studied excitons in this semiconductor, a quadrupole polariton is relatively unexplored since its first discovery using coherent quantum beat spectroscopy [Frohlich *et al.* (1991); Langer *et al.* (1995)]. The measured lifetime of quadrupole polaritons is about 2 ns and this much longer lifetime arises from the above noted dipole-forbidden nature of Cu_2O. Being a coherent quantum superposition of a quadrupole exciton and a photon, this

quasiparticle can be selectively created via resonant excitation. We have recently shown its unique half-matter/half-light characteristics such as scattering by atomic-scale impurities [Jang & Ketterson (2007)], significantly reduced Auger-type collisional loss [Jang & Ketterson (2008); Mani *et al.* (2010)], and resonantly enhanced reflection [Jang *et al.* (2008b)] at the crystal boundary, as demonstrated by the series of low-temperature PL experiments under resonant two-photon excitation. Together with dephasing times of several nanoseconds, these findings suggest that high-density quadrupole polaritons can be effectively confined to achieve polariton lasing and possibly "thermodynamic" BEC of polaritons.

Renewed interest in Cu_2O has been generated with thermal-oxidation-based fabrication of high-quality synthetic crystals with various morphologies [Mani *et al.* (2009a)] and observation of a very strong third-order optical nonlinearity supported by both Z-scan and third harmonic generation (THG) at room temperature [Mani *et al.* (2009b)]. Considering that the first-leading nonlinear term is the third order due to the centrosymmetric crystal structure of Cu_2O, this semiconductor, when engineered into unconventional structures, can be a very attractive system for optoelectronic applications involving various third-order nonlinear optical processes especially in the mid-IR range. Emerging practical examples involving coherent mid-IR applications are sensing for organic and inorganic molecules for environmental issues [Pestov *et al.* (2008); Pushkarsky *et al.* (2006)], minimal invasive medical surgery [Serebryakov *et al.* (2010)], and direct imaging of biological structures [Zipfel *et al.* (2003a)]. Also, Cu_2O has been considered an active material for solar cell applications [Olsen *et al.* (1982)].

This chapter is organized as follows: In Sec. 2 we describe fundamental properties of excitonic matter in Cu_2O. In Sec. 3 we describe the preparation method for high-quality synthetic Cu_2O crystals and the experimental setup for the measurements. In Sec. 4 typical two-photon generation of quadrupole polaritons is examined based on the relevant selection rules. In Sec. 5 we report on unique properties of quadrupole polaritons arising from their half-matter/half-light characters. In Sec. 6 we discuss quadrupole polariton generation under external mechanical stress and separate two-beam techniques. In Sec. 7 various nonlinear optical processes in Cu_2O are investigated and we propose a new direction for polariton-based BEC in this semiconductor. Section 8 gives our summary and conclusions.

2. Properties of excitonic matter in Cu_2O

The "cuprite" crystal structure of Cu_2O consists of interpenetrating bcc (O) and fcc (Cu) sublattices [see Fig. 1(a)]. The Bravais lattice is simple cubic with a lattice constant of 0.43 nm [Dahl & Switendick (1966)]. Due to the *center of inversion* around each copper atom site, both the lowest conduction band ($^2\Gamma_6^+$) built from Cu 4*s* levels and the highest valence band ($^2\Gamma_7^+$) from Cu 3*d* levels have a positive parity at zone center, causing a *dipole-forbidden energy gap* of $E_g = 2.17$ eV [Grun *et al.* (1961)]. The next highest valence band ($^4\Gamma_8^+$) lies 130 meV lower due to the spin-orbit interaction. The second lowest conduction band ($^4\Gamma_8^-$), lying 450 meV above the lowest conduction band, serves as an intermediate state for various optical-phonon-assisted recombination processes. Figure 1(b) schematically illustrates the band structure of Cu_2O at zone center when considering only two conduction and two valence bands that form the visible exciton series. Therefore, there are four possible exciton series referred to as "yellow" ($^2\Gamma_6^+ \otimes {}^2\Gamma_7^+$), "green" ($^2\Gamma_6^+ \otimes {}^4\Gamma_8^+$), "blue" ($^4\Gamma_8^- \otimes {}^2\Gamma_7^+$), and "indigo" ($^4\Gamma_8^- \otimes {}^4\Gamma_8^+$). Our primary concern is *dipole-forbidden yellow* exciton ($^2\Gamma_6^+ \otimes^2 \Gamma_7^+$), which is the bound state of an

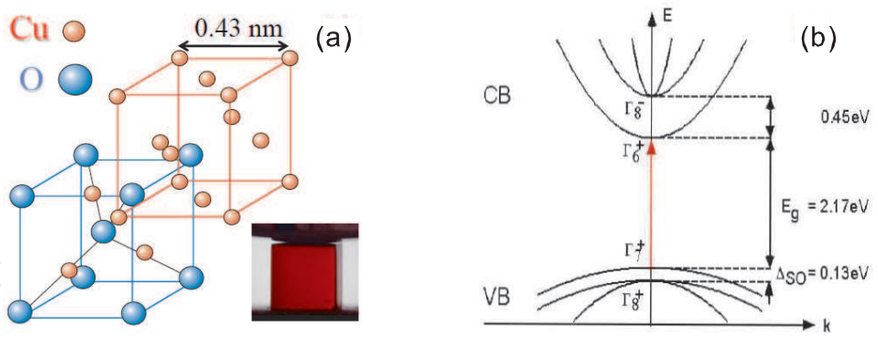

Fig. 1. (a) Crystal structure of Cu_2O. Inset: natural-growth bulk Cu_2O crystal. (b) Schematic of the Cu_2O band structure near zone center. The red arrow denotes quadrupole transition.

electron in the lowest conduction band ($^2\Gamma_6^+$) and a hole in the highest valence band ($^2\Gamma_7^+$), and shows a hydrogenic Rydberg series in the optical absorption spectrum [Hayashi & Katsuki (1952)]. Including so-called central cell corrections [Kavoulakis *et al.* (1997)], a spectroscopic fit to the observed Rydberg series reveals a tightly bound 1s excitonic state with a binding energy of 153 meV, corresponding to Bohr radius of 0.7 nm. The measured translational mass of the exciton is about $2.7m_e$, where m_e is the electron mass [Yu & Shen (1975)].

Since both the conduction and valence bands each have a simple spin-up/spin-down degeneracy, an exciton has a four-fold degeneracy, which is split into a triply-degenerate "$J = 1$" *orthoexciton* ($^3\Gamma_{25}^+$) and a nondegenerate "$J = 0$" *paraexciton* ($^1\Gamma_2^+$) by the electron-hole exchange interaction. The measured exchange splitting energy is 12 meV, the paraexciton level lying lowest [Kuwabara *et al.* (1977)]. Direct transition to the orthoexciton state is quadrupole allowed, but strictly forbidden for the paraexciton state because the process requires spin flip. Spin exchange between these two exciton states is possible via emission or absorption of a single transverse acoustic (TA) phonon [Jang *et al.* (2004); Wolfe & Jang (2005)]. Recently, Dasbach *et al.* (2004) performed high-resolution spectroscopy and observed the fine splitting of the triplet orthoexciton levels into the so-called "dark" and "bright" states depending on the wavevector direction inside the crystal. Although the relevant splitting is very small (several μeV), this fine structure of orthoexciton states crucially affects both one- and two-photon selection rules [Dasbach *et al.* (2004); Inoue & Toyozawa (1965); Jang *et al.* (2008a); Yoshioka & Kuwata-Gonokami (2006)].

Near the light cone ($k \simeq 2.63 \times 10^5$ cm^{-1}), only a bright orthoexciton quadrupole couples to the electromagnetic field, resulting in a quadrupole polariton. This is a coherent quantum superposition of a bright orthoexciton (matter) and a photon (light) field. The corresponding modes involve two branches which, depending on the wavevector, are either exciton-like or photon-like. This quasiparticle can be most simply described by coupled exciton-photon wave equations in momentum-energy ($\mathbf{k}, \omega$) space [Hopfield (1958)]:

$$\hbar\omega\hat{a}_{\mathbf{k}} = \hbar v k\hat{a}_{\mathbf{k}} + \eta^*\hat{b}_{\mathbf{k}}, \tag{1}$$

$$\hbar\omega\hat{b}_{\mathbf{k}} = \left(\frac{\hbar^2k^2}{2m} + E_o - i\Gamma\right)\hat{b}_{\mathbf{k}} + \eta\hat{a}_{\mathbf{k}}, \tag{2}$$

where $\hat{a}_{\mathbf{k}}$ and $\hat{b}_{\mathbf{k}}$ ($\propto e^{-i\omega t}$) are the photon and exciton annihilation operators, v is the velocity of light in the medium, m is the exciton mass, E_o is the internal energy of an exciton, and

Γ is a phenomenological damping rate. Equations (1) and (2) denote the photonic and excitonic parts of a polariton wave, where the coupling coefficient η is proportional to k for a quadrupole exciton. The solution to the above equations yields the quadrupole polariton dispersion [see Fig. 12(b)]. The propagating nature of the quadrupole polariton was first observed in the variation of the beat period using coherent quantum beat spectroscopy under resonant one-photon excitation [Frohlich *et al.* (1991); Langer *et al.* (1995)]. By contrast, a dark orthoexciton does not directly couple to the radiation field. When both excitonic matter species are generated under resonant excitation, the initial coherence of the laser light is essentially carried by them. These resonantly created dark orthoexcitons and quadrupole polaritons are potentially important in semiconductor-based coherent quantum information science [Yoshioka & Kuwata-Gonokami (2006)].

Excitons in Cu_2O can be created by conventional one-photon over-the-gap excitation. Under this excitation condition, electron-hole (*e-h*) pairs are initially generated which subsequently combine to form excitons via a screened Coulomb interaction. This "nonresonant" excitation results in excitons that initially have an excess kinetic energy and the exciton gas temperature can be much higher than the lattice temperature. Both orthoexcitons and paraexcitons can recombine via *indirect* phonon-assisted processes [Elliot (1961); Petroff *et al.* (1975)], but only the bright orthoexciton states can radiatively recombine by *direct* quadrupole transition, displaying a sharp Lorentzian peak.[1] Due to the flat dispersion relation of optical phonons, the phonon-assisted PL line can sample excitons having all possible kinetic energies, yielding a kinetic energy distribution of excitons [Beg & Shapiro (1976)]. At temperatures lower than about 20 K, the lifetime of orthoexcitons is basically limited by down-conversion into lower-lying paraexcitons, which is on the order of several nanoseconds [Jang *et al.* (2004); Wolfe & Jang (2005)]. Paraexcitons can have a lifetime up to several milliseconds in high-purity natural-growth samples but is extrinsically limited by the impurity concentration, i.e., the sample quality [Jang *et al.* (2006)]. Most of the previous experiments directed at excitonic BEC in Cu_2O were carried out using one-photon excitation [Fortin *et al.* (1993); Hulin *et al.* (1980); Snoke *et al.* (1987; 1990); Snoke & Negoita (2000); Wolfe *et al.* (1995)].

In contrast, quadrupole polaritons can be generated using *resonant* excitation involving either one or two photons [Frohlich *et al.* (1991); Goto *et al.* (1997); Ideguchi *et al.* (2008); Jang & Ketterson (2007); Jang *et al.* (2008a); Langer *et al.* (1995); Sun *et al.* (2001); Tayagaki *et al.* (2006)]. Rather than trying to cool the highly nonequilibrium state which follows nonresonant excitation, thermalization of the system under resonant excitation involves a subsequent *heating* induced by acoustic phonon absorption. Once resonantly generated, the lifetime (total coherence time) of quadrupole polaritons is basically limited by various elastic and inelastic dephasing processes [Takagahara (1985)]. Inelastic energy relaxation processes include irreversible damping arising from radiative recombination, thermalization to orthoexcitons, down-conversion to paraexcitons, and capture by ambient impurities, whereas elastic processes are caused by pure transverse dephasing mechanisms, affecting the phase only. All excitons and quadrupole polaritons undergo a *density-dependent* Auger-type decay process at high densities [Jang & Ketterson (2008); Tayagaki *et al.* (2006)]. According to the recent model [Jang & Wolfe (2005; 2006a;c)], it seems to arise due to formation of *optically inactive* biexcitons though their existence has not been confirmed spectroscopically yet.

[1] Details on various relaxation processes of excitons in Cu_2O are discussed in Jang (2005).

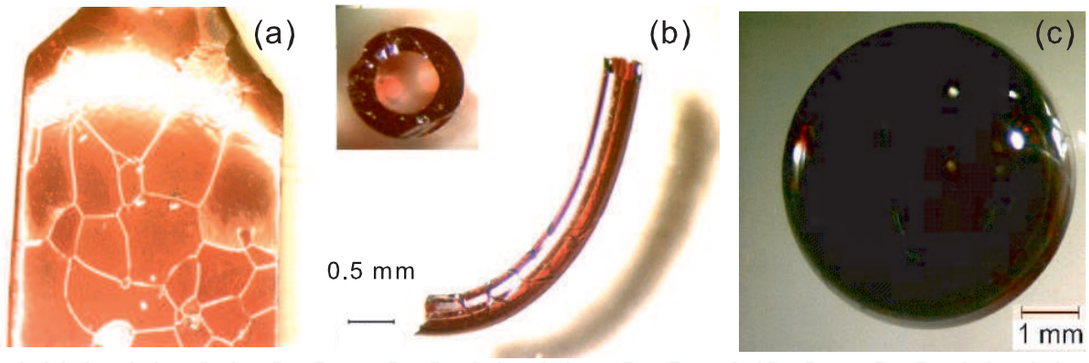

Fig. 2. High-quality synthetic crystals of Cu_2O grown by thermal oxidation with various structures: (a) Platelet with macroscopic grain boundaries, (b) hollow cylinder (inset: cross section), and (c) spheroid.

3. Experimental methods

In order to obtain shiny, ruby-red colored, large-area single crystals of Cu_2O, we utilize conventional thermal oxidation of metallic Cu with platelet, wire, and shot structures followed by a high-temperature annealing protocol. The oxidation parameters and annealing procedure are obtained from Toth *et al.* (1960) and carefully adjusted to refine the Cu_2O crystal quality. During the growth process, we carefully maintain O_2 pressure and temperature to lie within the middle of the Cu_2O phase in the $Cu-Cu_2O-CuO$ phase diagram [Schmidt-Whitley *et al.* (1974)]. It is noted that elevated annealing temperatures near the melting temperature of Cu_2O and slower rates of oxidation, annealing, and cooling of the samples play key roles in diminishing the concentration of macroscopic defects such as voids and CuO precipitates.[2] Figure 2 shows as prepared, (a) platelet, (b) hollow tube, and (c) spherical structures of Cu_2O, respectively. It is interesting that the oxidation of Cu wire at high temperatures leads to the formation of *hollow* tubules of Cu_2O. Together with a spheroid form, such unconventional structures could be utilized to confine propagating quadrupole polaritons within a whispering gallery mode [Vollmer & Arnold (2008)]. Our natural-growth samples used in the experiments were donated by the Smithsonian Institute.

Our one- and two-photon experiments are performed on both natural-growth and synthetic Cu_2O crystals. For resonant two-photon excitation, the samples are properly oriented relative to the laser polarization (**E**-field direction) to maximize optical transition. The cryogenic temperatures are produced with a Janis variable-gas-flow optical cryostat and an accompanying temperature controller. We use the frequency-tripled output of a mode-locked Nd:YAG laser (EKSPLA PL 2143 series) with a pulse width of about 30 ps and a repetition rate of 10 Hz in order to synchronously pump an optical parametric amplifier (OPA). The OPA generates vertically polarized pulses in the range of 400 - 2000 nm. At the two-photon resonance energy ϵ_{2p} = 1016.5 meV (1219.4 nm), the spectral bandwidth of the laser light from the OPA is rather broad, about 8 meV full width at half maximum. However, the phase space compression phenomena [Kuwata-Gonokami *et al.* (2002)] ensure an effective creation of quadrupole polaritons or dark orthoexcitons since the lower energy portions $(\epsilon_{2p} - \delta\epsilon_{2p})$ are exactly compensated by higher parts $(\epsilon_{2p} + \delta\epsilon_{2p})$, thereby satisfying both energy and

[2] See Mani *et al.* (2009a) for detailed growth procedures and X-ray and optical characterizations.

Table 1: Selection rules along (100)

State	1-photon	2-photon
O_{xy}	$\cos^2\theta$	0
O_{yz}	0	$\sin^2 2\theta$
O_{zx}	$\sin^2\theta$	0

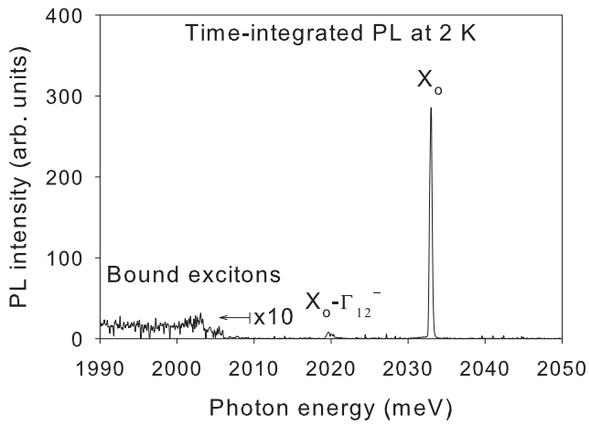

Fig. 3. Time-integrated PL spectrum at 2 K under resonant two-photon excitation along a (100) direction that initially generates dark orthoexcitons. The bound exciton PL is $\times 10$ magnified.

momentum conservations. In order to verify the one- and two-photon selection rules, a pair of polarization analyzers is placed in front of and behind the samples. The incident laser pulse is focused onto a spot 500 μm in diameter using a 15 cm focal-length lens. The PL from excitonic matter is collected and focused onto a fiber optic bundle mounted on a goniometer, thereby allowing us to measure the angular dependence (ϕ) of the PL. The output of the fiber optic bundle is coupled to the entrance slit of a Spex Spec-One 500 M spectrometer and detected using a nitrogen-cooled CCD camera. The collection efficiency of our optical system as a function of the collection angle ϕ is explained in Jang & Ketterson (2007).

The Z-scan technique is traditionally employed to probe the third-order nonlinearity $\chi^{(3)}$ by translating a test sample through the beam waist of a focused Gaussian-laser profile and measuring the corresponding variation of the transmitted beam intensity in the far field [Sheik-Bahae *et al.* (1990; 1991)]. For our Z-scan experiments [Mani *et al.* (2009b; 2010)], the laser pulses from the OPA is first *spatially* filtered using a 100 μm pinhole, insuring transmission of only the TEM_{00} Gaussian mode. This Gaussian beam is focused on Cu_2O using a converging lens with a 7.5 cm focal length, which is mounted on a computer-controlled stage that is translated relative to the window of the optical cryostat. This allows us to continuously change the input irradiance I as a function of the lens position Z; I can be varied more than a factor of 400 simply by translating Z in our 1-inch scan range. The change in the far-field image of the transmitted beam with Z is minimized by using a combination of collection lenses prior to entering a photomultiplier tube (PMT). The output of the PMT is fed into a boxcar integrator and read out using a data acquisition system.

4. Resonant two-photon excitation and selection rules

According to **k**-dependent exchange interactions [Dasbach *et al.* (2004)], two-photon excitation along highly symmetric crystal orientations does not generate quadrupole polaritons but dark orthoexcitons. For example, Table 1 shows the selection rules for a (100) direction, ensuring that two-photon excitation along this direction initially creates dark orthoexcitons, the O_{yz} state, whose one-photon transition is not allowed. This can be a crucial issue for achieving a polariton-based whispering gallery mode, where the direction of the

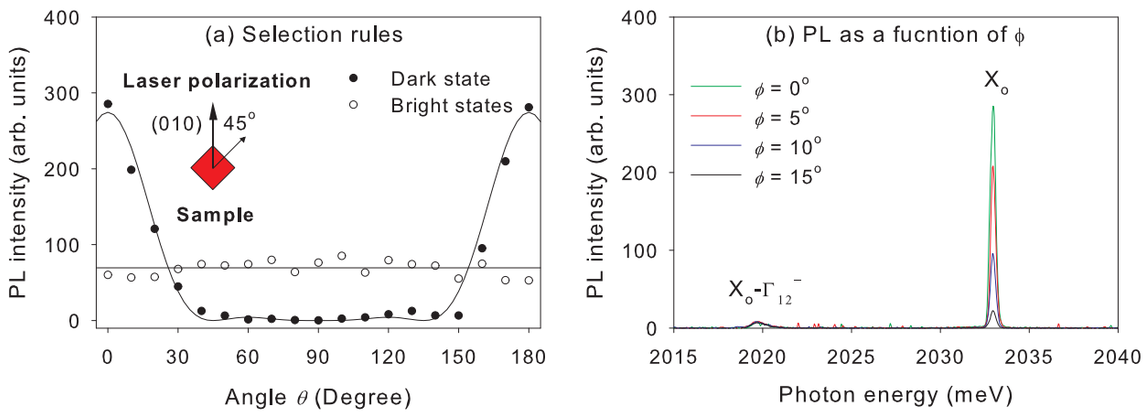

Fig. 4. (a) Dots (circles) correspond to the observed polarization dependence of the X_o line obtained using analyzers in front of (behind) the sample. Superimposed solid curve (line) is the two-photon (one-photon) selection rules. Inset: schematic of the excitation geometry. (b) Time-integrated PL spectra at 2 K as a function of the collection angle $\phi = 0, 5, 10$, and 15°.

polariton propagation is arbitrarily reflected and guided by curved interfaces. However, quadrupole polaritons can be *indirectly* generated although dark states are initially created. Figure 3 shows a typical time-integrated PL spectrum under resonant two-photon excitation at 2 K along a (100) direction. Considering that optically inactive "singlet" O_{yz} dark orthoexcitons are initially generated in this excitation geometry, it seems rather surprising to observe several PL lines. Once created, however, these excitons undergo various relaxation processes and can recombine accompanied with the emission of a single photon. For example, they can: (i) inelastically scatter from optical phonons, causing the phonon replica ($X_o - \Gamma_{12}^-$), (ii) be captured by ambient impurities, where the symmetry of an exciton is broken and the parent selection rules do not apply, resulting in the broad bound exciton PL, and (iii) convert into the bright orthoexciton states that directly recombine, yielding a sharp X_o line. They also can either nonradiatively decay due to phonon cascade or down-convert into the lower-lying paraexcitons. Compared with other inelastic energy relaxation processes that cause irreversible damping of dark orthoexcitons, we find that the conversion into the bright state is the most dominant mechanism based on the observed strong X_o line.

In order to verify that the direct X_o line arises from two bright "doublet" O_{xy} and O_{zx} states, which are subsequently converted from the dark "singlet" state, we examine the one- and two-photon selection rules using two analyzers. The dots in Fig. 4(a) correspond to the observed two-photon selection rules for dark orthoexcitons inferred from the bright-state PL (X_o line) obtained with the analyzer in front of the sample. Considering that the sample orientation is 45° as shown in the inset of Fig. 4(a), the overall two-photon polarization dependence is shown as the solid curve and is given by $P_{2p} \propto \sin^2[2(\theta - 45^o)]\cos^4\theta$, where the extra $\cos^4\theta$ term accounts for two-photon excitation of the incident laser intensity that decreases with $\cos^2\theta$, as the analyzer rotates from $\theta = 0^o$. The circles correspond to the observed one-photon selection rules for bright orthoexcitons, converted from dark orthoexcitons, obtained with the analyzer behind the sample. Note that the measured X_o intensity barely depends on the analyzer angle. Considering the total polarization of the two bright states, $O_{xy} \propto \cos^2\theta$ and $O_{zx} \propto \sin^2\theta$, this implies that the two-fold degenerate bright states are *equally* populated: $P_{1p} \propto \cos^2\theta + \sin^2\theta =$ constant [solid line in Fig. 4(a)]. Clearly,

the observed polarization dependencies support that the strong direct PL line arises from *dark-to-bright conversion*.

This dark-to-bright conversion was first observed by Yoshioka & Kuwata-Gonokami (2006) using two-photon absorption along the (110) direction, and the measured conversion rate was about 5 ns^{-1}. The contribution to this conversion rate due to phonon scattering can be estimated by the deformation potential theory [Trebin *et al.* (1981); Waters *et al.* (1980)]:[3]

$$\gamma(T) = \frac{\Xi_{xy}^2 m^2 \delta}{3\pi\rho v_T \hbar^4} \left(1 + \frac{2k_B T}{v_T\sqrt{2m\delta}}\right), \tag{3}$$

where $\Xi_{xy} = 0.18$ eV is the shear deformation potential, $m = 2.7m_e$ is the exciton mass, $\rho = 6.1$ g/cm^3 is the mass density of Cu_2O, and $v_T = 1.3$ km/s is the TA-phonon velocity. With the measured splitting $\delta = 2\,\mu$eV along this direction [Dasbach *et al.* (2004)], Eq. (3) yields a conversion rate $\gamma \simeq 0.7 \times 10^{-4}$ ns^{-1} at 2 K. This implies that dark-to-bright conversion via phonon scattering is negligible. Therefore, it most likely arises from state mixing caused by the so-called *cross relaxation*, where two dark states *elastically* scatter to equally populate two bright states by satisfying angular momentum conservation. Although the dark orthoexcitons may lose their initial coherence, this implies that their phase information can be partially carried by subsequently generated bright states, because elastic scattering only induces a phase shift in the total ensemble coherence [Takagahara (1985)]. This cross relaxation mechanism is currently under investigation using two-photon quantum beat spectroscopy as a function of the incident laser intensity.

Figure 4(b) shows the PL spectra under the same conditions for several collection angles ϕ in the range of $0 - 15^o$, where ϕ is the angle between the laser beam direction and the PL collection direction. Note that the direct PL intensity sharply depends on ϕ and is well correlated with the laser-propagation direction, whereas the indirect phonon line does not; i.e. it is essentially isotropic. This clearly indicates that the initial momentum of a dark orthoexciton inherited from the laser is nearly conserved after the conversion. This leads the momentum of a subsequently generated bright orthoexciton being near the light cone to form a quadrupole polariton, which propagates along the initial laser direction. Based on highly directional PL properties, this strongly indicates that propagating quadrupole polaritons are *indirectly* generated. This implies that two-photon excitation in Cu_2O eventually generates quadrupole polaritons regardless of the crystal orientation.

5. Half-matter/half-light characteristics of quadrupole polaritons

Near the quadrupole resonance in Cu_2O, light propagating through the medium is accompanied by quadrupolar polarization through the excitonic component. Ideally, the angular distribution of the quadrupole polariton PL should be same as the angular divergence for the incident laser because its propagation direction is inherently determined by the incident laser direction. However, these quadrupole polaritons can lose their initial coherence because the excitonic component of the mode, a tightly bound *e-h* pair, is subject to wide-angle scattering by atomic-scale imperfections within the crystal. Therefore, we employ angle-resolved spectroscopy to examine scattering by ambient impurities, which results in decoherence, and monitor the angular divergence of quadrupole polaritons generated

[3] See, for example, Jang & Wolfe (2006b) for the derivation of the rate due to off-diagonal shear scattering.

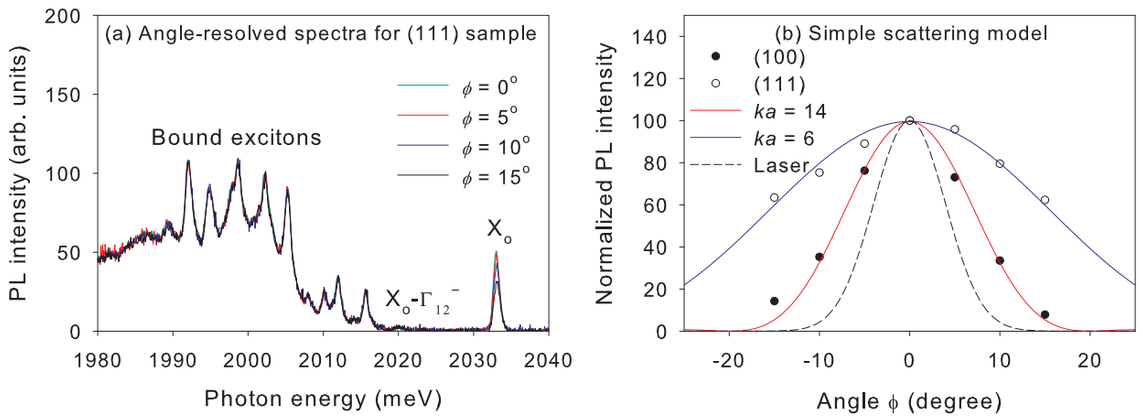

Fig. 5. (a) Time-integrated PL spectra at 2 K as a function of $\phi = 0, 5, 10$, and 15° obtained from the (111) oriented sample. (b) Angular distributions of the X_o intensities from the (100)-cut (dots) and (111)-cut (circles) samples, respectively. The solid red and blue curves correspond to our simplified model for $ka = 14$ and 6. The dashed curve denotes the angular distribution of the transmitted laser measured just below the quadrupole resonance.

by resonant two-photon transition. In fact, Fig. 4(b) displays such angle-resolved spectra obtained from a (100)-cut sample for several collection angles. This angle dependence can differ from sample to sample.

Figure 5(a) plots time-integrated spectra obtained from a (111)-cut sample[4] under the same conditions as Fig. 4(b). For this direction, the observed X_o line is caused by quadrupole polaritons both directly and indirectly generated by two-photon absorption. The series of peaks in a range from 1980 to 2015 meV arise from excitons bound to ambient impurities that are essentially isotropic (no ϕ dependence). Considering much enhanced bound exciton PL intensity, this sample apparently contains more impurities and the X_o intensity from quadrupole polaritons remaining after transmission through the sample is strongly attenuated due to ambient impurity scattering. This is clearly indicated by much more gradual drop in the X_o intensity as ϕ changes from 0°, compared with that in Fig. 4(b). This implies that the photonic character (straight propagation with a definite $\mathbf{k}$) of a quadrupole polariton is obstructed by impurities, significantly affecting its excitonic component and thus deflecting its initial path which, in turn, affects the photonic component by the exciton-photon coupling terms in Eqs. (1) and (2).

From the fact that this wide-angle impurity scattering originates from the *particle nature* of a quadrupole polariton, our problem reduces to a "propagating" (not diffusive[5]) exciton that is most likely scattered by ambient *charged* impurities. The 1*s* exciton is uncharged and has no higher multipole moments. However, a charged impurity can induce a dipole moment in the excitonic part of a quadrupole polariton. The potential between an *induced* dipole and an ion has the form $V(r) = -\alpha e^2/2r^4$ for large r, where α is the polarizability [Landau & Lifshitz (1977)]. But the scattering amplitude calculated with this potential is divergent due to the behavior of $V(r)$ at small r. To avoid this problem we assume the interaction approaches a

[4] This sample contains high impurity levels and was used for studying bound excitons [Jang *et al.* (2006)].
[5] Highly diffusive nature of excitons in Cu_2O are described in Trauernicht & Wolfe (1986).

constant at small r. Including a phenomenological "cutoff radius" a, the model potential is

$$V(r) = -\frac{\alpha e^2}{2r^4} \quad (r > a) \text{ and } V_o \equiv -\frac{\alpha e^2}{2a^4} \quad (r < a). \tag{4}$$

Since the observed angular divergence depends on the impurity concentration, the trajectory of a quadrupole polariton is mainly determined by successive small-angle scattering, leading to a Gaussian-like distribution. In order to obtain the angular distribution due to multiple scattering, one needs to numerically add each stochastic process considering many parameters [Amsel *et al.* (2003)]. In the absence of information on the nature and distribution of the scattering centers we model the behavior as arising from single scattering events which are parameterized by a cutoff radius a. By neglecting the long-range contribution, which is very small compared with the one for $r < a$, the quantum mechanical scattering amplitude produced by Eq. (4) is given in the first-order Born approximation by

$$f(\Omega) = -\frac{2m'}{\hbar^2}\frac{V_o}{q}\int_0^a r\sin(qr)dr = -\frac{2m'}{\hbar^2}\frac{V_o}{q^3}\{\sin(qa) - qa\cos(qa)\}, \tag{5}$$

where we take m' to be the effective mass of a quadrupole polariton and $q = |\mathbf{k} - \mathbf{k}'| = 2k\sin(\theta/2)$ is the associated momentum transfer with the incident wavevector $\mathbf{k}$. Since the interaction potential is spherically symmetric, the scattering amplitude $f(\Omega) = f(\theta)$ does not contain any azimuthal-angle dependence. The corresponding differential cross section is analytic and given by the absolute square of the scattering amplitude. The observed angular distribution is then proportional to this differential cross section.

In Fig. 5(b), we plot the angular distributions of the quadrupole polariton PL intensities from Figs. 4(b) (dots) and 5(a) (circles), where these intensity distributions are normalized at $\phi = 0^o$ for comparison. The superimposed fits are generated using our model potential with $ka = 14$ (red) and 6 (blue), respectively. The dashed curve is the angular divergence of the incident laser. Note that the only adjustable parameter is the effective screening radius a since the wavevector of a quadrupole polariton is given by $k \simeq 2.63 \times 10^5$ cm^{-1} with a minor spreading Δk, which is a measure of the polariton bottleneck. Although our model might oversimplify the light character of a quadrupole polariton that actually undergoes multiple scattering, therefore affecting macroscopic ensemble coherence in a complicated way, we believe that it captures the essence of the dominant polariton-impurity scattering mechanism, where the charged-impurity concentration is parameterized by a cutoff radius a. Obviously, a stronger X_o signal with a narrower angular distribution would occur for samples containing lower impurity level. This also implies that the total coherence time can be extrinsically limited by scattering from impurities. Minimizing such extrinsic effects is crucial for preserving coherence. This angle-resolved technique can also be used as a sensitive path-averaged (and by some deconvolution perhaps a local) impurity detector allowing some degree of optimization for the coherence time of propagating quadrupole polaritons.

Another striking effect[6] arising from the dual character of quadrupole polaritons is anomalous Fresnel coefficients at the quadrupole resonance, resulting in resonantly enhanced reflection of quadrupole polaritons at crystal boundaries [Jang *et al.* (2008b)]. As originally suggested by

[6] Unlike polaritonic effects discussed in this section, which result from the half-matter character, suppressed collisional loss of quadrupole polaritons arises basically due to their half-light character and this is discussed in Sec. 7.

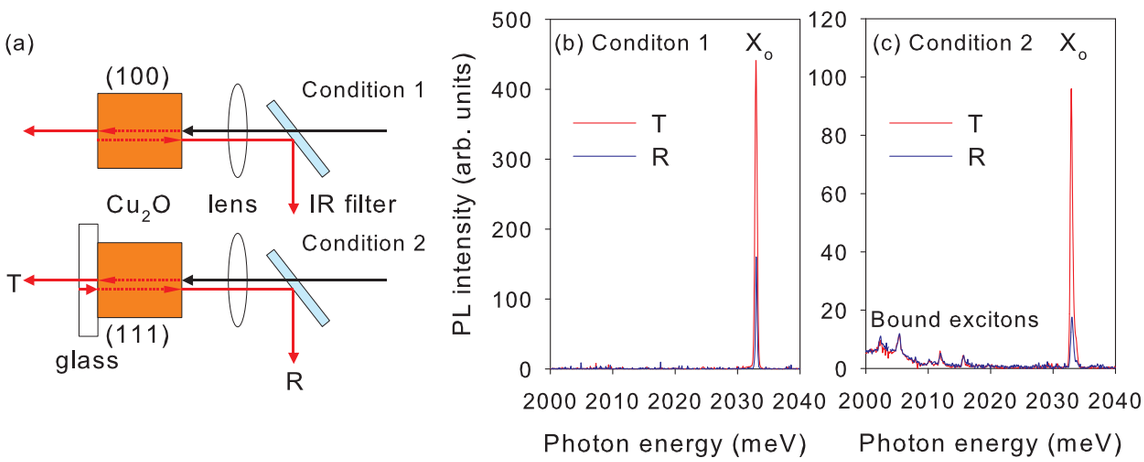

Fig. 6. (a) Schematic diagram of the PL collection geometry for two different boundary conditions. The incident IR beam (solid arrows) excites Cu_2O to create a traveling quadrupole polariton wave (red dashed arrows) inside the medium via two-photon absorption. As this wave leaves Cu_2O, it converts into photons (red solid arrows), yielding PL signals that we detect. The time-integrated PL measured from the incoming surface R (blue trace) and the opposite surface T (red trace) under (b) condition 1 and (c) condition 2, respectively.

Hopfield & Thomas (1963), polariton propagation in a dielectric medium is rather different from classical light propagation. The complexity basically arises from the fact that there are two propagating modes in the crystal associated with upper- and lower-branch polaritons. Therefore, the usual Maxwell boundary conditions are not enough to determine the field amplitudes for these two modes, requiring so-called *additional boundary conditions*. The special case of quadrupole polaritons was theoretically studied by Pekar *et al.* (1981) assuming a Frenkel-type excitation that vanishes at the vacuum-crystal boundary. However, the correction to the "effective" index of refraction at the quadrupole resonance is predicted to be negligible due to relatively small quadrupole coupling. In order to check this resonance effect, we experimentally investigate the "total" reflectance (R) and transmittance (T) of traveling quadrupole polaritons arising from multiple internal reflections at the sample surfaces. In our excitation geometry, we define R and T as the X_o intensities collected from the incoming and the opposing (outgoing) surfaces, respectively [see Fig. 6(a)]. Surprisingly, our principal finding indicates that the experimental value of T/R at the quadrupole resonance differs significantly from the prediction of Pekar *et al.* (1981).

Figure 6(a) shows a schematic diagram for measuring R and T for the two boundary conditions using (100)- and (111)-oriented natural-growth samples, respectively. Since we use resonant two-photon excitation in which the excitation energy is the half of the quadrupole polariton energy, the measured PL is decoupled from the incident laser. In order to measure R we use a dichroic mirror, which is an efficient IR filter transmitting the excitation light but reflecting visible light. The measured reflectivity in our observation range (1980 – 2040 meV) is about 0.485. Two-photon generated quadrupole polaritons propagate through the crystal along the incident laser direction. Therefore, the *opposite surface* is the first boundary encountered. For condition 2, the sample is attached to a glass slide to impose a different boundary condition. In this case, there is one more interface formed by the

glass and the superfluid He bath. When the quadrupole polariton wave leaves Cu_2O, it is converted into transmitted light and a portion of that is reflected from this extra boundary by satisfying *usual* Fresnel relations. These reflected photons will resonantly excite Cu_2O via *one-photon* excitation at the glass and Cu_2O interface, thereby producing a counterpropagating quadrupole polariton wave in Cu_2O.

In Fig. 6(b) we plot the observed PL spectrum (red trace) for condition 1 as collected from the opposite surface, corresponding to T. The blue trace shows the light transmitted at the incoming surface (corrected for the reflectivity of the IR filter), corresponding to R. The measured T/R is about 2.75 ± 0.05. Considering multiple internal reflections, this ratio can be analytically calculated and is given by

$$\frac{T}{R} = \frac{(te^{-\gamma})[1 + (re^{-\gamma})^2 + \ldots]}{(re^{-\gamma})(te^{-\gamma})[1 + (re^{-\gamma})^2 + \ldots]} = \frac{1}{re^{-\gamma}}, \tag{6}$$

where $e^{-\gamma}$ is a phenomenological damping factor which includes all irreversible losses during a "one-way trip", and r and t are the reflection and transmission coefficients at the Cu_2O and superfluid He interface, which are approximately given by

$$r = \left(\frac{n-1}{n+1}\right)^2 \quad \text{and} \quad t = \frac{4n}{(n+1)^2}. \tag{7}$$

Note that R in Eq. (6) contains t because of transmission at the incoming surface. Also, Eq. (6) shows that the measured T/R is only affected by a *single* damping factor because the accumulative damping due to multiple internal reflections exactly cancels out in this ratio. In fact, $e^{-\gamma}$ is negligible for our relatively thin samples ($d < 1$ mm) considering a much longer decoherence length $l = v_g\tau \simeq 2 - 20$ mm, where v_g is the quadrupole polariton group velocity (on the order of $10^6 - 10^7$ m/s) and $\tau \simeq 2$ ns is the measured decoherence time [Frohlich *et al.* (1991)]. Assuming $e^{-\gamma} = 1$ and using $n = 2.65$ for Cu_2O, the simple Fresnel prediction yields $T/R = 4.89$, which does not agree with our measurement. Note that this damping factor, if significant, induces a larger discrepancy between the theoretical and measured T/R.

Figure 6(c) plots the measured R and T for condition 2 in which the sample attached to the glass contains a higher impurity concentration as indicated by the bound exciton PL. The isotropic bound exciton PL from two different collections overlap each other, verifying the scaling factor introduced by the IR filter. Because of an extra boundary formed by the glass and superfluid He, there are numerous combinations of multiple reflections and transmissions. In our analysis, we consider up to the 4th order, involving 8 combined reflections and transmissions at the boundaries. Using the measured index of refraction for the glass, $n_g = 1.48$, the calculation yields $T/R = 9.77$. However, the measured T/R for the condition 2 is about 5.46 ± 0.15, again significantly different from the classical Fresnel prediction.

The present theory [Pekar *et al.* (1981)] based on the additional boundary conditions predicts a *slight* modification in the effective index of refraction n_{eff} for a propagating quadrupole polariton wave depending on the wavevector direction. For example, n_{eff} for normal incidence is given by

$$n_{eff} = \sqrt{\varepsilon + \frac{2m'}{\hbar^2}\frac{4\pi q^2}{\Omega}} \equiv \sqrt{\varepsilon + \frac{1}{\zeta}}, \tag{8}$$

where $\varepsilon = 7$ is the background dielectric constant, m' is the effective mass for a quadrupole polariton that depends on the wavevector direction, q is the exciton quadrupole moment, and Ω is the unit-cell volume. The microscopic calculation yields $1/\zeta \simeq -0.46$ and -0.17 for (100) and (111) directions, respectively. Therefore, the predicted index of refraction at the quadrupole resonance is about $n_{eff} = \sqrt{7 - 0.46} \simeq 2.56$ for the (100) direction. This negligible correction apparently does not explain our measurements and n_{eff} must be significantly larger than $n = 2.65$. Based on the series of experiments, we have confirmed that our experimental results can be explained by introducing the effective index of refraction $n_{eff} = 4.0 \pm 0.1$ for the boundary conditions we employed. This increased index of refraction in turn implies a significantly enhanced reflection of quadrupole polaritons at the crystal boundary.

The failure of the present theory might result from assuming localized Frenkel excitons, whereas Cu_2O is well known for hosting weakly bound Mott-Wannier excitons. Alternatively, the amplitude of the orthoexciton may not vanish at the boundary as discussed below. This significantly enhanced reflection arises most likely from the behavior of the matter component (exciton). Although thermal excitons may break down at the crystal boundary, the quasi-ballistic excitonic component of moving quadrupole polaritons will most likely be reflected at the surface with minimal surface recombination, presumably hindering quadrupole polaritons from exiting Cu_2O and thus causing enhanced reflection. In the absence of a proper theory, we propose that the phase shift associated with this reflection be regarded as a free parameter. It may be that the behavior can be Fresnel-like, however with a modified index of refraction. We believe that this anomalous reflection is universal, arising from the half-matter/half-light property of polaritons, regardless of host materials. Our results have implications for the optoelectronic design of polariton waveguides and resonators in which a larger (effective) index of refraction implies a larger angle of total internal reflection which in turn affects the cutoff wavelength and with it the confinement of polaritons inside the medium.

6. Efficient quadrupole polariton generation with unconventional approaches

As a bound state of an electron and a hole, an exciton in Cu_2O is electrically neutral and only weakly magnetic.[7] Therefore, conventional electromagnetic external perturbations do not cause a significant modification in its electronic properties. But, mechanical strain affects the electronic states of Cu_2O in two ways: (i) it induces a bandgap shift and, more important, (ii) it lowers the crystal symmetry, resulting in splitting of orthoexciton levels depending on the stress direction. Although numerous studies on excitons under external stress were performed [Jang & Wolfe (2006b); Lin & Wolfe (1993); Liu & Snoke (2005); Mysyrowicz *et al.* (1983); Naka & Nagasawa (2002); Snoke & Negoita (2000); Trauernicht & Wolfe (1986)], the effect of external stress on quadrupole polaritons is essentially a virgin territory, potentially full of unexplored interesting physics.

Under spatially inhomogeneous Hertzian stress [Snoke & Negoita (2000)], a strain well forms a potential minimum for excitons inside the crystal. This technique has been extensively used in attempts to create trapped high-density excitons. Figures 7(a) and (b) illustrate the potential well formed in a Lucite crystal under Hertzian contact stress and a schematic of

[7] One needs more than 10 T to observe noticeable exciton-level splitting in Cu_2O induced by external magnetic field [Fishman *et al.* (2009)].

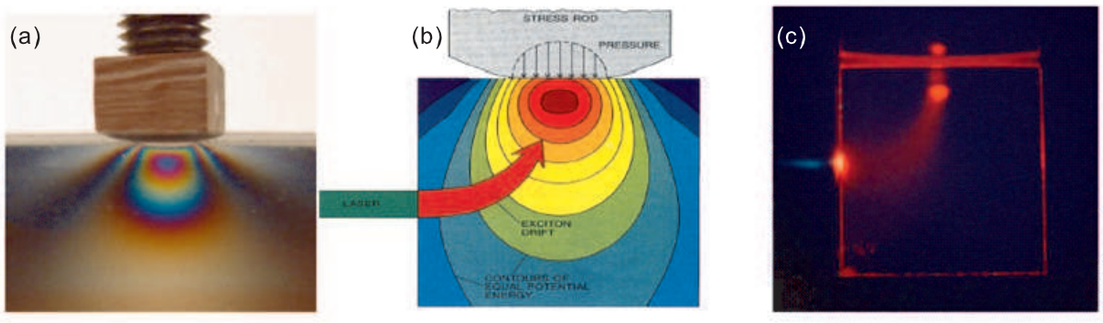

Fig. 7. (a) Hertzian contact at Lucite showing potential minimum and equipotential contours monitored by cross polarizer. (b) Schematic of potential-trap experiments and (c) image of excitons in Cu_2O effectively confined by a potential well just below the stressor after fast drift from the excitation spot (left).

stress experiments at low temperatures, respectively. Exciton drift into such a potential well in Cu_2O at 2 K is clearly shown in Fig. 7(c). One can then ask how this harmonic potential well affects the propagating quadrupole polaritons. They could be attracted by the well due to the excitonic component, as shown in Fig. 7(c), or not because the photonic component is little affected. It will be interesting to study the influence of the potential well on the quadrupole polariton propagation.

As a preliminary, we first conduct a rather simple experiment using *uniaxial* stress along a (001) direction and collect the PL from a (110) surface of a natural-growth Cu_2O sample.[8] Surprisingly, our results indicate that the quadrupole polariton PL (X_o line) is significantly enhanced with external stress. Figures 8(a)−(c) plot the observed X_o intensities (red traces) as a function of stress in the range of $\sigma = 0 - 0.3$ kbar. The heavy solid traces are fits using a single or double Gaussian function, considering the spectral resolution of our detection system. As we increase stress, the triply-degenerate quadrupole state splits into the singlet and doublet states where the latter lies lower [Jang & Wolfe (2006b)]. The measured splitting is consistent with our theoretical prediction. In Figs. 8(d)−(f), we plot the corresponding polarization dependence of the X_o intensities obtained using an analyzer behind the sample, indicating a significant modification of the one-photon selection rules. Most of all, it is very interesting that the quadrupole polariton PL rapidly increases with σ and its brightness at σ = 0.3 kbar is more than 10 times that obtained under no stress. We have also performed the same experiments using one-photon over-the-gap excitation to check the *exciton* PL as a function of σ and confirmed that no such a strong enhancement is observed. It implies that this is solely related to either "coherent" polaritonic effects or enhanced two-photon excitation, arising from modification of the electronic structure (mixing between dark and bright states) induced by external stress. In order to clarify the underlying mechanism, one needs to time-resolve the population and relaxation dynamics of quadrupole polaritons as a function of σ. Clearly, this stress technique is promising for generating high-density quadrupole polaritons for BEC.

Previous experiments based on two-photon absorption were conducted using a single-beam laser tuned to the two-photon quadrupole resonance (1219.4 nm). However, quadrupole polariton generation can be also accomplished using two independent beam sources as long as (i) the sum of beam frequencies matches with the quadrupole resonance and (ii) the

[8] This sample was previously used for studying paraexcitons under stress [Trauernicht & Wolfe (1986)].

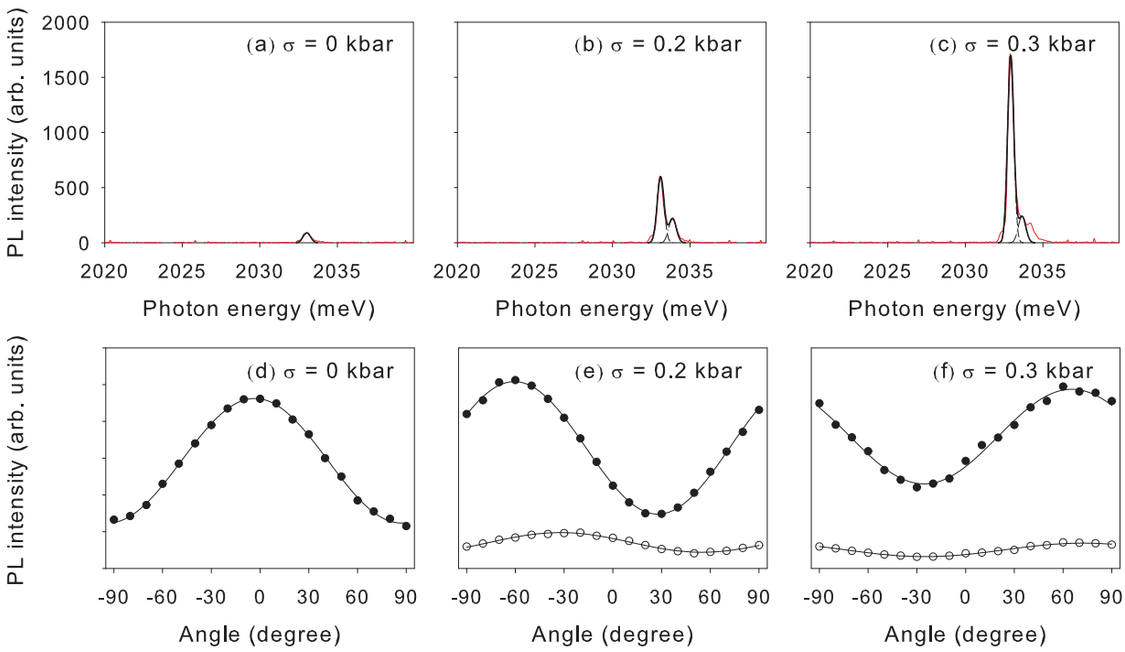

Fig. 8. Time-integrated quadrupole polariton PL (red traces) at (a) $\sigma = 0$ kbar, (b) 0.2 kbar, and (c) 0.3 kbar, respectively, superimposed with Gaussian fits (heavy solid curves). (d) Measured polarization dependence (dots) under no stress, well explained by the one-photon selection rules (solid curve). The corresponding polarization dependence under external stress are plotted by dots (doublet) and circles (singlet) in (e) and (f). Superimposed are empirical fits.

conservation of momentum is fulfilled inside the crystal (phase matching). This two-beam technique has been initially triggered by the idea of mixing much stronger pulses from the pump YAG laser (1064 nm) and those from the OPA (tuned to 1428 nm) in order to generate high-density quadrupole polaritons. Moreover, we can independently control the polarizations of the two incident beams and their propagation directions, and therefore, the resulting wavevector of quadrupole polaritons inside the sample.

Unlike one-beam two-photon technique, however, there are number of issues to optimize two-beam two-photon excitation such as pulse synchronization, OPA wavelength tuning, and precise optical alignments, etc. For example, the dots in Fig. 9(a) correspond to the quadrupole polariton signal when the delay arm of the OPA is varied near the pulse synchronization position. The superimposed curve is a fit to the data, yielding a temporal overlap of 30 ps, which is consistent with the pulse widths of two beams. In Fig. 9(b), we plot the quadrupole polariton signal (dots) observed when we vary the wavelength of the OPA near 1428 nm. The solid curve is a fit that basically reflects the spectral linewidth of the OPA at this wavelength. These clearly show that two-beam two-photon efficiency strongly depends on both time and wavelength detuning of the OPA. The dots (and superimposed curve) in Fig. 9(c) show the relative polarization dependence of the two-beam two-photon efficiency when the polarization angle of the OPA is varied in the range from -90^o to 90^o, indicating that orthogonal polarization is not favorable, as expected. Employing this two-beam two-photon technique, we can also study "impact ionization" of quadrupole polaritons by varying two incident beam powers independently, which arises from additional absorption

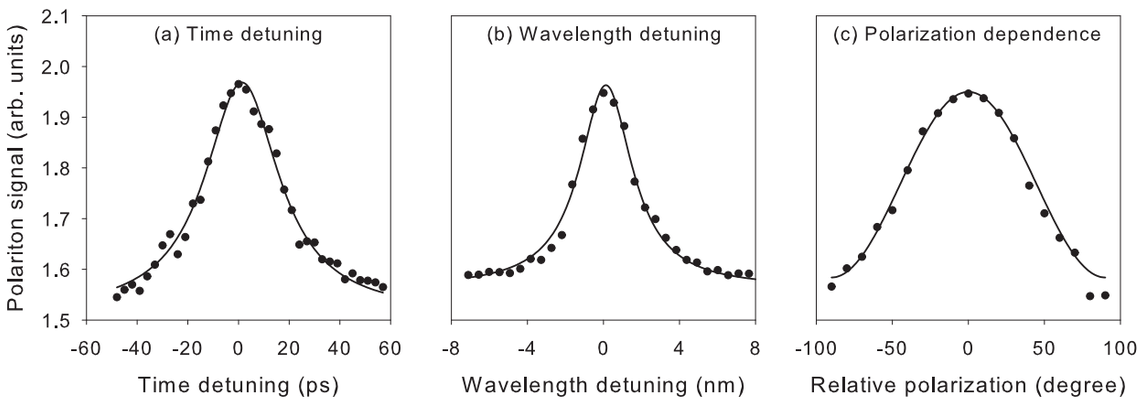

Fig. 9. Measured X_o intensity from quadrupole polaritons as a function of (a) OPA time detuning, (b) OPA wavelength detuning, and (c) OPA polarization relative to the fixed vertical polarization of the 1064 nm output from the YAG laser, respectively.

of an incident photon by a quadrupole polariton that ionizes the excitonic component. In fact, this mechanism can mimic Auger-type collisional loss of quadrupole polaritons, and therefore, measuring and controlling this process could be an important issue for achieving a high-density polariton system.

Another interesting direction is to use "quadrupole-induced" second harmonic generation (SHG) to efficiently generate high-density quadrupole polaritons using a *non-collinear orthogonal polarization geometry* [Figliozzi *et al.* (2005)]. Interestingly, the corresponding SHG polarization is largest when the incident electric fields are mutually orthogonal and is proportional to $\sin\psi$, where ψ is the angle between two wavevectors inside the crystal. This condition is quite different from that for two-beam two-photon absorption as explained above. The technique was developed to investigate the surface structure of Si nanocrystals embedded in SiO_2 matrix using SHG signals, which is enhanced by several orders of magnitude [Figliozzi *et al.* (2005)]. Since Cu_2O has a centrosymmetric crystal structure, SHG is not viable in the dipole approximation. However, one can turn on SHG in this semiconductor by exploiting this technique. Clearly, it is an interesting question whether quadrupole polariton generation can be further improved via enhanced quadrupole SHG.

7. Third-order nonlinearity and nonlinear processes at quadrupole resonance

Although Cu_2O has a rich history as a prototype material for studying fundamental exciton physics, its nonlinear optical properties have received little attention presumably because of its vanishing second-order susceptibility $\chi^{(2)}$ stemming from its centrosymmetric crystal structure. Consequently, the lowest-order optical nonlinearity in Cu_2O arises from the third-order susceptibility $\chi^{(3)}$. Precise characterization of the nonlinear optical parameters such as $\chi^{(3)}$ and the two-photon absorption coefficient β is crucial in evaluating its potential for nonlinear optical applications and estimating the densities of excitonic matter under two-photon excitation. Recently, we have reported the first measurement of the nonlinear refractive index $n_2 \propto \mathrm{Re}[\chi^{(3)}/n]$ $(n = 2.65)$ and β based on the Z-scan technique [Mani *et al.* (2009b)].

The single-beam Z-scan technique relies on the phenomenon of self-focusing of an intense Gaussian laser beam in the presence of a nonlinear medium [Sheik-Bahae *et al.* (1990; 1991)].

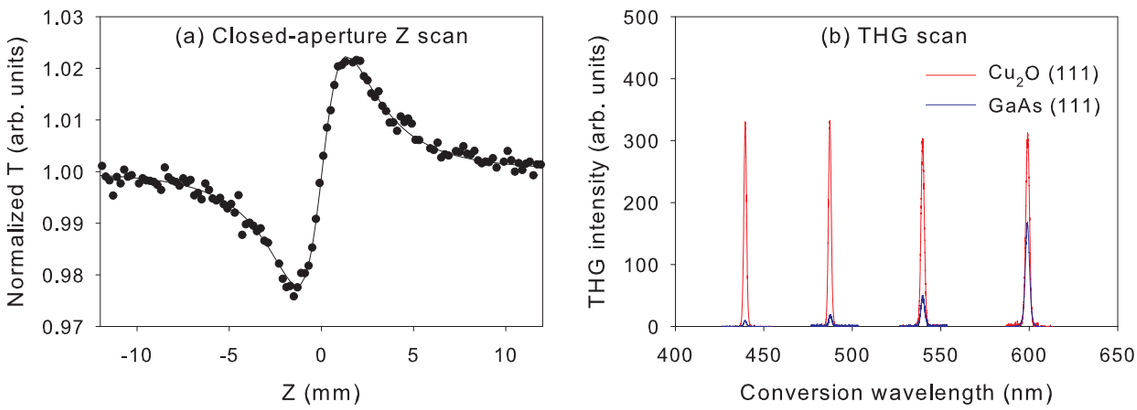

Fig. 10. (a) Normalized closed-aperture Z-scan data (dots) obtained from a (110)-oriented natural-growth Cu_2O sample with 20% aperture transmittance, superimposed by a theoretical fit (solid trace). (b) Wavelength-dependent THG from Cu_2O (red) and GaAs (blue).

One can characterize both n_2 and β using the closed- and open-aperture Z-scan configurations, respectively. The dots in Fig. 10(a) correspond to the normalized closed-aperture Z-scan trace showing a valley-peak configuration, indicating positive nonlinearity of Cu_2O, when the on-axis irradiance at the focus is set to $I(Z = 0) = 0.86$ GW/cm^2 at $\lambda = 1064$ nm. At this relatively low irradiance level, with negligible *e-h* pair generation by two-photon transition, the closed-aperture Z-scan accounts for purely refractive nonlinearity due to the bound electronic Kerr effect; $\Delta n = n_2 I$, where Δn is the on-axis index change at focus. Transmittance change at the detector (ΔT) is related to Δn by

$$\Delta T \simeq 0.406(1-S)^{0.25}\frac{2\pi}{\lambda}d_{eff}\Delta n, \tag{9}$$

where $S = 20\%$ is the aperture transmittance and $d_{eff} = (1-e^{-\alpha d})/\alpha$, with the linear absorption coefficient $\alpha = 47$ cm^{-1} at $\lambda = 1064$ nm for the sample thickness $d = 100$ μm. The solid curve is a least-square fit to the data, yielding $n_2 = 1.32 \times 10^{-10}$ esu. We have found that similar values of n_2 are obtained from our synthetic samples [Mani *et al.* (2009b)]. This measured n_2 value of Cu_2O seems comparable with those of other conventional nonlinear semiconductors with large n_2 values. However, it is important to note that $n_2 \propto 1/E_g^4$, where E_g is the bandgap, and that the best $\chi^{(3)}$ materials have bandgap energies far below that for Cu_2O [see for example Table III of Sheik-Bahae *et al.* (1991)]. This implies that the matrix elements entering $\chi^{(3)}$ are very large in Cu_2O but the overall response is scaled down by its relatively large bandgap energy. Considering this factor, we believe that Cu_2O is a potential $\chi^{(3)}$ material with a bandgap energy lying in the visible region.

This is further confirmed by Fig. 10(b), showing the measured THG signals from Cu_2O and GaAs, both oriented along a (111) direction and 0.5 mm thick, when the input OPA wavelength is varied from 1300 nm to 1800 nm. Considering that n_2 of GaAs is about two times that of Cu_2O, it is initially surprising that THG from Cu_2O is more intense. This basically arises from two reasons: (i) since $\chi^{(2)}$ of GaAs is very large, the incident laser most strongly contributes to the lower-order SHG process and (ii) GaAs is a dipole-allowed semiconductor in which

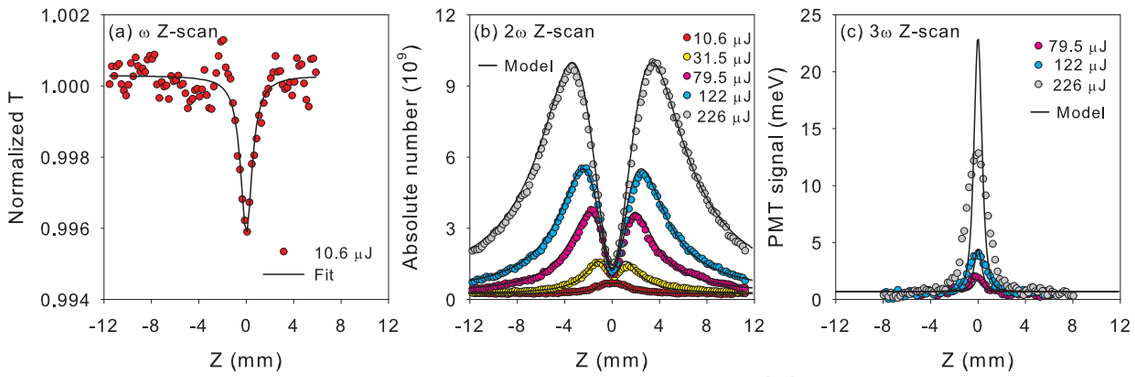

Fig. 11. (a) Normalized ω Z-scan (red dots) for 10 μJ/pulse, superimposed by a theoretical fit (solid trace) with $\beta = 0.217$ cm/GW. (b) 2ω Z-scan traces (colored dots) for various excitation levels in the range of $10.4 - 226$ μJ/pulse, fit by the theoretical model (solid traces). (c) 3ω Z-scan traces (colored dots) for 79.5, 122, and 226 μJ/pulse. The solid curves correspond to a model assuming no fundamental depletion.

the THG light being above the bandgap is strongly absorbed compared with the case for a dipole-forbidden semiconductor of Cu_2O. In support of the latter, Fig. 10(b) shows that the THG intensity from GaAs sharply depends on the OPA input wavelength, whereas for Cu_2O it does not. Most importantly, it is noteworthy that measurable THG signals can be transmitted through a 0.5 mm-thick Cu_2O sample used in the measurements since the absorption lengths for the converted THG wavelengths shown in Fig. 10(b) are known to be less than a few microns [O'Hara *et al.* (1999b)]. This implies that Cu_2O could be utilized for an active THG medium working at ω_{IR} in the mid-IR range such that $3\omega_{IR}$ is still below the bandgap of Cu_2O without any complication from $\chi^{(2)}$ contributions.

Recently, it has been suggested that three-photon excitation [Ideguchi *et al.* (2008)] and THG [Mani *et al.* (2009b)] can affect population dynamics of quadrupole polaritons in Cu_2O under strong two-photon excitation. Considering possible complications caused by these high-order processes, the feasibility of quadrupole polariton BEC remains an open question. In pursuit of this question we systematically investigate various nonlinear optical processes such as two-photon absorption, Auger-type recombination, and THG under resonant two-photon excitation at 2 K. By extending the standard *open-aperture* Z-scan method (that only monitors the intensity at ω), we also keep track of the frequency-doubled (2ω) and tripled (3ω) Z-scan outputs to probe the quadrupole polariton PL and THG responses using appropriate band-pass filters [Mani *et al.* (2010)].

In order to estimate the *absolute* number of quadrupole polaritons generated under two-photon excitation, it is essential to precisely determine β, basically arising from $\mathrm{Im}[\chi^{(3)}]$ at the quadrupole resonance. The red dots in Fig. 11(a) correspond to the normalized ω Z-scan trace, showing two-photon absorption for 10.4 μJ/pulse. Note that only 0.4% of the incident beam is absorbed at the focus ($Z = 0$). The solid trace is a theoretical fit [Sheik-Bahae *et al.* (1990)] with $\beta = 0.217$ cm/GW and the beam waist of $\omega_0 = 15.1$ μm at $Z = 0$. This ω_0 is consistent with the standard Gaussian width $\sigma_s = 0.19$ cm of the incident beam through $\sigma_s / f = \lambda / \pi\omega_0$, where $f = 7.5$ cm and $\lambda = 1219.4$ nm. Unlike conventional band-to-band two-photon absorption, the effect at the narrow quadrupole resonance depends on the spectral width $\delta\omega$ of the incident laser. In our case of $\delta\omega \simeq 8$ meV, we have confirmed

that $\beta = 0.217$ cm/GW within a 50% uncertainty based on the series of ω Z-scan experiments. We also find that the measured β value persists up to 226 μJ/pulse without any evidence for higher-order multiphoton absorption. This implies that one-photon transition induced by subsequent absorption of the THG light apparently mimics three-photon excitation.
With β determined, depletion of the fundamental intensity I along the beam path z due to two-photon absorption can be calculated and is given by

$$\frac{dI}{dz} = -\beta I^2 \rightarrow I(z;Z,t) = \frac{I_0(Z,t)}{I_0(Z,t)\beta z + 1}, \tag{10}$$

where $I_0(Z,t)$ is the photon flux at the incident sample surface, which is a function of the focusing lens position Z and given by

$$I_0(Z,t) = \frac{2P(t)}{\pi\omega^2(Z)} \rightarrow \frac{2P}{\pi\omega^2(Z)} = \frac{2P}{\pi\omega_0^2(1+Z^2/Z_0^2)}, \tag{11}$$

where $P(t)$ is the input pulse power with a 30 ps temporal profile and $Z_0 = \pi\omega_0^2/\lambda \simeq 0.06$ cm is the confocal parameter. Since Z-scan yields the time-averaged data, we use the *time-integrated* pulse power P to evaluate $I_0(Z)$. In Eq. (11), a factor of 2 is correctly introduced for the averaged power of the TEM_{00} mode Gaussian beam.
Figure 11(b) plots the 2ω Z-scan traces (colored dots) under several excitation levels from 10.4 μJ/pulse to 226 μJ/pulse, showing quadrupole polaritons generated by resonant two-photon excitation. Note that we plot the time-averaged *absolute* number of quadrupole polaritons using the measured β as explained below. As predicted for two-photon absorption in a finite-thickness sample, for a given excitation level, the measured quadrupole polariton number increases quadratically with the corresponding $I_0(Z)$ as we sweep Z.[9] However, a striking dip-like feature develops in the vicinity of $Z = 0$ as we increase the pulse energy and quadrupole polariton generation severely saturates at the focus. In order to check whether any signal was lost due to the finite aperture of the PMT collector, we have probed the quadrupole polariton spatial profile in the far field as a function of Z using a gated intensified CCD camera and verified that this mechanism is negligible [Mani *et al.* (2010)]. Together with ω Z-scan indicating negligible higher-order contributions, this implies that quadrupole polaritons undergo an Auger-type two-body decay process at high densities.
In order to explain 2ω Z-scan, we now model the population and relaxation dynamics of quadrupole polaritons. The quadrupole polariton generation rate G should match the laser absorption profile; $G(\mathbf{r};Z) = -(dI/dz)/2 = \beta I^2/2$, where a factor of $1/2$ accounts for energy conservation during two-photon absorption. The temporal behavior of the local quadrupole polariton density $n(\mathbf{r};Z,t)$ is described by

$$\frac{dn}{dt} = G(\mathbf{r};Z) - \frac{n}{\tau} - An^2, \tag{12}$$

where τ is the quadrupole polariton lifetime and A is an Auger coefficient [Jang & Wolfe (2005; 2006a;c); Jang & Ketterson (2008)]. The analytical solution to Eq. (12) exists and the

[9] If the sample is infinitely thick, the incident IR photons N should be all absorbed and the number of quadrupole polaritons created is simply $N/2$, independent of $I_0(Z)$.

time-averaged density $n(\mathbf{r};Z)$ is given by

$$n(\mathbf{r};Z) = \frac{\int n(\mathbf{r};Z,t)dt}{\int dt} = \frac{\ln[1+An_0(\mathbf{r};Z)\tau]}{A\tau}, \tag{13}$$

where the initial density is well approximated by $n_0(\mathbf{r};Z) = \{[1+4G(\mathbf{r};Z)A\tau_p^2]^{1/2}-1\}/2A\tau_p$ with the pulse width $\tau_p = 30$ ps. While n_0 is essentially $G\tau_p$ at low excitation, it approaches to $(G/A)^{1/2}$ and is limited by fast Auger-type decay during the 30 ps buildup time when $GA\tau_p^2 \gg 1$. To obtain the time-averaged quadrupole polariton number $N(Z)$ for a given Z, we numerically integrate $n(\mathbf{r};Z)$ over the sample dimension ($d = 100$ μm):

$$N(Z) = \int n(\mathbf{r};Z)d^3r = \pi\omega^2(Z)\int_0^d n(z;Z)dz. \tag{14}$$

Note that $N(Z)$ contains only two independent fit parameters of τ and A, since G is accurately determined with $\beta = 0.217$ cm/GW. The solid traces in Fig. 11(b) show $N(Z)$ using a single fit-parameter set of $\tau = 2$ ns and $A = 0.55\times10^{-16}$ cm^3/ns, showing excellent fits to the series of 2ω Z-scan data. A value $\tau = 2$ ns is consistent with that obtained from coherent quantum beat spectroscopy [Frohlich *et al.* (1991)] and A is about 2 times smaller than that reported based on Lyman absorption spectroscopy [Jang & Ketterson (2008); Tayagaki *et al.* (2006)].
Most of all, it is remarkable that the measured A value for quadrupole polaritons is more than 10 times *smaller* than that for thermalized excitons [Jang & Wolfe (2005; 2006a;c)]. This significantly reduced A seems puzzling but we can qualitatively explain it based on the unique property a quadrupole polariton possesses but an exciton does not. This two-body decay process for excitons is exclusively caused by "matter-matter collision" via Coulomb interaction between two *e-h* pairs consisting of two excitons. Since this process arises from random collision of excitons, it depends on the exciton *gas* temperature [Jang & Wolfe (2005; 2006a;c)]. However, as a quantum superposition of a photon (light) and a bright orthoexciton (matter), a quadrupole polariton also carries the *light* character that is not relevant to this collisional process. Unlike diffusive excitons, quadrupole polaritons all move in the same direction with a definite nonzero wavevector primarily determined by the incident laser beam. Therefore, they should have a greatly reduced probability for random collision. In this view, it is not surprising that quadrupole polaritons have a much suppressed Auger coefficient.
Figure 11(c) displays 3ω Z-scan traces (colored dots) for 79.5, 122, and 226 μJ/pulse, resulting from THG of the input laser. We confirmed that 3ω Z-scan responses were very small for lower excitation. Again, considering a submicron absorption length at 406.5 nm in Cu_2O, it is remarkable that measurable THG signals are transmitted through the sample. Since fundamental depletion due to two-photon absorption is negligible, the THG field intensity $E_{3\omega}$ as a function of Z is given by [Boyd (2008)]

$$E_{3\omega}(Z) = \frac{i3\omega}{2nc}\chi^{(3)}E^3(Z)J_{3\omega}(\Delta kd), \tag{15}$$

where n is the index of refraction for Cu_2O, c is the speed of light in vacuum, $E(Z) = [I_0(Z)/2nc]^{1/2}$, and $J_{3\omega}(\Delta kd)$ is the phase-matching factor. The solid traces in Fig. 11(c) are the predicted THG photon counting [$\propto \pi\omega^2(Z)|E_{3\omega}(Z)|^2$] properly scaled to match the overall data, simply assuming phase matching ($J_{3\omega} = d$) and using $I_0(Z)$ in Eq. (11). While this

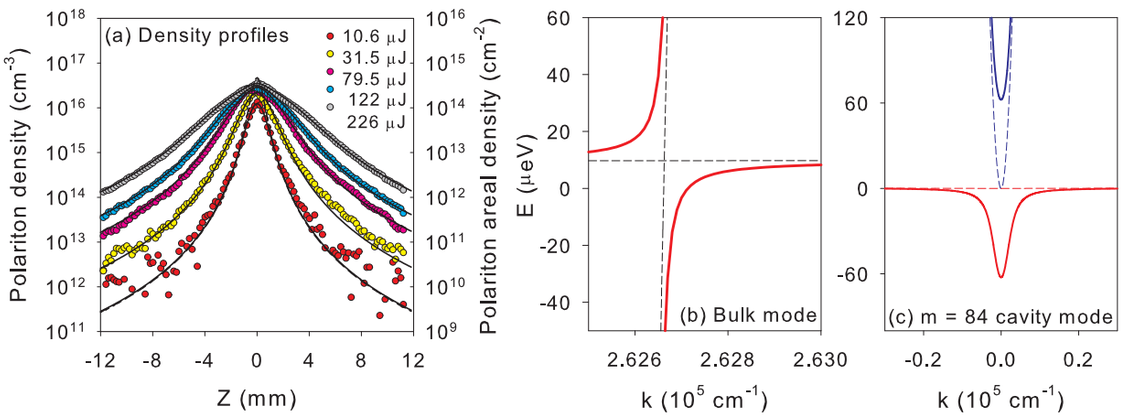

Fig. 12. (a) Time-averaged quadrupole polariton densities (colored dots) as a function of Z, superimposed by our Auger model (solid traces). Calculated quadrupole polariton dispersion for (b) 3D bulk and (c) 10 μm-thick cavity ($m = 84$) modes in Cu_2O for a (110) direction.

simple model basically corresponds to a I^3 fit, the observed 3ω Z-scan data reveal a different power dependence of $I^{1.8}$. We believe that this rather unusual power dependence stems from complicated processes involving (i) strong absorption of THG beam that crucially affects phase coherence between the fundamental and THG lights inside Cu_2O and/or (ii) possible contribution due to the generation of higher harmonics. Although a full understanding of detailed THG mechanism in Cu_2O awaits more experimental and theoretical studies, it is clear that high-density quadrupole polariton generation is more affected by an Auger-type process rather than THG, as indicated by our Auger model explaining 2ω Z-scan data without a $\chi^{(3)}$ parameter [see Fig. 11(b)].

Unlike typical dipole coupling encountered in other semiconductors, quadrupole coupling near the crossover is much smaller in bulk Cu_2O, causing relatively large curvature of the dispersion near the quadrupole polariton bottleneck; the associated group velocity is relatively fast and the effective mass is very small, several orders of magnitude smaller than the exciton mass [see Fig. 12(b)]. This should result in a significant reduction in the BEC transition density. Furthermore, the Auger-type cross section is significantly reduced for quadrupole polaritons owing to their half-matter/half-light characters. This implies that the experimentally achievable quadrupole polariton densities can be well above the critical density for BEC.

In order to estimate experimental quadrupole polariton densities attainable, we plot the time-averaged density $n(Z) = N(Z)/\pi\omega^2(Z)d$ (colored dots) in Fig. 12(a) using $N(Z)$ in Fig. 11(b). The solid traces correspond to our Auger model with $A = 0.55 \times 10^{-16}$ cm^3/ns. In our excitation range, the spatial extent of quadrupole polaritons along the propagation direction is limited by the sample thickness of $d = 100$ μm, which is smaller than the two-photon absorption length $(\beta I)^{-1}$. The corresponding areal densities $N(Z)/\pi\omega^2(Z)$ are also plotted in Fig. 12(a). Despite considerable decrease in $N(Z)$ around $Z = 0$ in Fig. 11(b), it is important to note that the maximum density still locates at the focus in which it saturates around 3×10^{16} cm^{-3} under high excitation levels. This is more than 10 times higher than the maximum thermal exciton density ($\simeq 10^{15}$ cm^{-3}) [O'Hara & Wolfe (2000)], basically due to the suppression of A by the same amount.

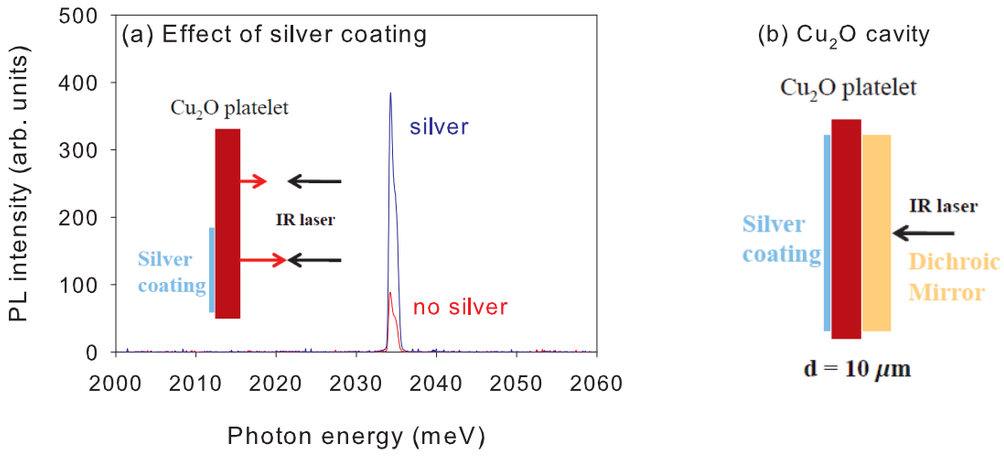

Fig. 13. (a) Time-integrated PL recorded using a reflection geometry, showing effective confinement of quadrupole polaritons from a silvered region . Inset depicts the sample and collection geometry. (b) Schematic diagram for a Cu_2O Fabry-Perot cavity.

Although the areal densities for quadrupole polaritons we observe in Cu_2O are much higher than the critical BEC density ($\simeq 10^9$ cm^{-2}) in the 2D cavity-polariton structures [Balili *et al.* (2007); Deng *et al.* (2003); Kasprzak *et al.* (2006)], BEC is not expected to arise in practice, since the *absence of a local minimum* precludes condensation as shown in Fig. 12(b); of course such minima have been engineered into the polariton dispersion curves of the 2D microcavities. This limitation might be circumvented by depositing partially transmitting mirrors on opposing sides of a flat platelet of Cu_2O, thereby forming a Fabry-Perot cavity [see Fig.13(b)]. In Fig. 12(c), we plot our simulation result for the $m = 84$ cavity-photon mode assuming a 10 μm-thick Cu_2O platelet that forms a Fabry-Perot cavity (blue dashed curve) sitting just above the exciton mode (red dashed curve).[10] Then, the lower-polariton branch (red solid curve) would develop a local minimum via quadrupole coupling associated with a very small effective mass ($\simeq 10^{-5} m_e$) in which long-lived quadrupole polaritons can condense.

Recently, we have experimentally confirmed that depositing a silver film on Cu_2O significantly enhances the quadrupole polariton confinement without altering underlying excitonic structures, as demonstrated by Fig. 13(a). The quadrupole polariton PL from a silvered region (blue trace) is about 4 times stronger than that from an unsilvered region (red trace). This behavior persists when we move the excitation position around the silvered portion. Figure 13(b) illustrates a detailed schematic of the proposed cavity system for quadrupole polariton BEC. The excitation surface of a Cu_2O platelet is attached to a commercial dichroic mirror that transmits the incident excitation beam in the IR (1219.4 nm), but strongly reflects the quadrupole polariton PL in the visible range (609.7 nm), thereby forming a *high-Q cavity with efficient quadrupole polariton generation*. Optimally coupling the OPA output to the cavity poses a more challenging problem, as it requires a way to continuously vary this coupling. We have two strategies for matching of mode frequency

[10] Smaller node numbers and large mode spacings would require a thinner sample. A promising technology to make thin Cu_2O films showing sharp exciton lines was reported by Markworth *et al.* (2001).

either by (i) adjusting the propagation direction of quadrupole polaritons relative to the plane normal or (ii) placing a silver mirror on the far side of the sample with a variable thickness. Unlike our previous experiments based on time-integrated methods, we plan to directly time-resolve the population and relaxation dynamics of two-photon generated quadrupole polaritons as a function of the input IR power and the angle of incidence. This will clearly reveal not only the impact of two-body decay on high-density quadrupole polaritons but also the coherent temporal evolution of long-lived quadrupole polariton condensate once achieved.

8. Concluding remarks

The goal of this chapter is to study both fundamental and technological aspects of natural-growth/synthetic cuprous oxide (Cu_2O) crystals that host long-lived excitonic matter and exhibit large third-order nonlinear optical responses. All these remarkable physical properties primarily originate from the centrosymmetric crystal structure and the dipole-forbidden bandgap of Cu_2O. Bright orthoexcitons intersecting the light cone quadrupole couple to the electromagnetic field and split into two polariton branches. A quadrupole polariton in Cu_2O is special in that it propagates over a macroscopic distance with a very long coherence time, compared with polaritons in conventional dipole-allowed semiconductors.

Based on the series of experiments under resonant two-photon excitation, we have demonstrated various interesting phenomena essentially arising from unique half-matter/half-light characteristics of quadrupole polaritons. However, our current understanding of the properties of a quadrupole polariton is rather empirical and accessible only experimentally, calling for a more rigorous microscopic description of this quasiparticle. More importantly, our findings imply that high-density quadrupole polaritons can be effectively confined inside Cu_2O and we have proposed a promising direction for long-lived polariton Bose-Einstein condensation (BEC). Clearly, BEC in a forbidden-gap semiconductor would be a valuable addition to the current BEC class from the perspective of fundamental physics. Also, polariton BEC on the order of several nanoseconds at nominal cryogenic temperatures will be a revolutionary step toward quantum computers and information sciences.

Various nonlinear optical parameters have been quantitatively characterized using Z-scan and third harmonic generation (THG) techniques. Distinctive and interesting properties of this semiconductor allow us to consider possible optoelectronic applications involving polariton-based waveguides and whispering gallery resonators, polariton lasers, and active third-order nonlinear optical devices. We have also discussed a set of particularly interesting and timely issues. This includes detailed research directions such as (i) high-density quadrupole polariton dynamics near BEC regime, (ii) impact of external stress on quadrupole polaritons, (iii) nonlinear optics at the quadrupole resonance using both two-beam two-photon absorption and quadrupole-induced second harmonic generation, and (iv) clarification of underlying THG mechanism.

9. Acknowledgments

The author acknowledges the essential collaboration of J. B. Ketterson at Northwestern University, S. Mani at Intel Corporation, and J. P. Wolfe at the University of Illinois. This work is supported by the National Science Foundation under (i) the Northwestern Materials Research Center; Grant DMR-0520513, (ii) the U.S./Ireland cooperation; Grant 0306731, and (iii) the Integrative Graduate Education and Research Training program; Grant 0801685.

10. References

Amsel, G.; Battistig, G. & L'Hoir, A. (2003). Small angle multiple scattering of fast ions, physics, stochastic theory and numerical calculations, *Nucl. Instrum. Methods Phys. Res. B* 201, 325.

Balili, R.; Hartwell, V.; Snoke, D.; Pfeiffer, L. & West, K. (2007). Bose-Einstein condensation of microcavity polaritons in a trap, *Science* 316, 1007.

Beg, M. M. & Shapiro, S. M. (1976). Study of phonon dispersion relations in cuprous oxide by inelastic neutron scattering, *Phys. Rev. B* 13, 1728.

Boyd, R. W. (2008). *Nonlinear Optics*, 3rd ed. Academic Press, San Diego. pp. 119.

Christopoulos, S.; von Hogersthal, G. B. H.; Grundy, A. J. D.; Lagoudakis, P. G.; Kavokin, A. V.; Baumgerg, J. J.; Christmann, G.; Butte, R.; Feltin, E.; Carlin, J. -F. & Grandjean, N. (2007). Room-temperature polariton lasing in semiconductor microcavities, *Phys. Rev. Lett.* 98, 126405.

Dahl, J. P. & Switendick, A. C. (1966). Energy bands in cuprous oxide, *J. Phys. Chem. Solids* 27, 931.

Dasbach, G.; Frohlich, D.; Klieber, R.; Suter, D.; Bayer, M. & Stolz, H. (2004). Wave-vector-dependent exchange interaction and its relevance for the effective exciton mass in Cu2O, *Phys. Rev. B* 70, 045206.

Deng, H.; Weihs, G.; Snoke, D.; Bloch, J. & Yamamoto, Y. (2003). Polariton lasing vs. photon lasing in a semiconductor microcavity, *Proc. Natl. Acad. Sci. U.S.A.* 100, 15318.

Deng, H.; Haug, H. & Yamamoto, Y. (2010). Exciton-polariton Bose-Einstein condensation, *Rev. Mod. Phys.* 82, 1489.

Elliot, R. J. (1961). Symmetry of excitons in cuprous oxide, *Phys. Rev.* 124, 340.

Figliozzi, P.; Sun, L.; Jiang, Y.; Matlis, N.; Mattern, B.; Downer, M. C.; Withrow, S. P.; White, C. W. & Mendoza, B. S. (2005). Single-beam and enhanced two-beam second-harmonic generation from silicon nanocrystals by use of spatially inhomogeneous femtosecond pulses, *Phys. Rev. Lett.* 94, 047401.

Fishman, D.; Faugeras, C.; Potemski, M.; Revcolevschi, A. & van Loosdrecht, P. H. M. (2009). Magneto-optical readout of dark exciton distribution in cuprous oxide, *Phys. Rev. B* 80, 045208.

Fortin, E.; Farfard, S. & Mysyrowicz, A. (1993). Exciton transport in Cu_2O: Evidence for excitonic superfluidity?, *Phys. Rev. Lett.* 70, 3951 and references therein.

Frohlich, D.; Kulik, A.; Uebbing, B.; Mysyrowicz, A.; Langer, V.; Stolz, H. & von der Osten, W. (1991). Coherent propagation and quantum beats of quadrupole polaritons in Cu_2O, *Phys. Rev. Lett.* 67, 2343.

Goto, T.; Shen, M. Y.; Koyama, S. & Yokouchi, T. (1997). Bose-Einstein statistics of orthoexcitons generated by two-photon resonant absorption in cuprous oxide, *Phys. Rev. B* 55, 7609.

Grun, J. B.; Seiskind, M. & Nikitine, S. (1961). Etude spectrophotometrique des spectres continus de Cu_2O a diverses temperatures, *J. Phys. Chem. Solids* 19, 189.

Hayashi M. & Katsuki, K. (1952). Hydrogen-like absorption spectrum of cuprous oxide, *J. Phys. Soc. Jpn.* 7, 599.

Hopfield, J. J. (1958). Theory of the contribution of excitons to the complex dielectric constant of crystals, *Phys. Rev.* 112, 1555.

Hopfield, J. J. & Thomas, D. G. (1963). Theoretical and experimental effect of spatial dispersion on the optical properties of crystals, *Phys. Rev.* 132, 563.

Hulin, D.; Mysyrowicz, A. & Benoit a la Guillaume, C. (1980). Evidence for Bose-Einstein statistics in an exciton gas, *Phys. Rev. Lett.* 45, 1970.

Ideguchi, T.; Yoshioka, K.; Mysyrowicz, A. & Kuwata-Gonokami, M. (2008). Coherent quantum control of excitons at ultracold and high density in Cu_2O with phase manipulated pulses, *Phys. Rev. Lett.* 100, 233001.

Inoue, M. & Toyozawa, Y. (1965). Two-photon absorption and energy band structure, *J. Phys. Soc. Jpn.* 20, 363.

Jang, J. I.; O'Hara, K. E. & Wolfe, J. P. (2004). Spin-exchange kinetics of excitons in Cu_2O: Transverse acoustic phonon mechanism, *Phys. Rev. B* 70, 195205.

Jang, J. I. & Wolfe, J. P. (2005). Biexcitons in the semiconductor Cu_2O: An explanation of the rapid decay of excitons, *Phys. Rev. B* 72, 241201(R).

Jang, J. I. (2005). Lifetimes of excitons in cuprous oxide, *Ph.D. thesis*, University of Illinois.

Jang, J. I. & Wolfe, J. P. (2006). Exciton decay in Cu_2O at high density and low temperature: Auger recombination, spin-flip scattering, and molecule formation, *Solid State Commun.* 137, 91.

Jang, J. I. & Wolfe, J. P. (2006). Relaxation of stress-split orthoexcitons in Cu_2O, *Phys. Rev. B* 73, 075207.

Jang, J. I. & Wolfe, J. P. (2006). Auger recombination and biexcitons in Cu_2O: A case for dark excitonic matter, *Phys. Rev. B* 74, 045211.

Jang, J. I.; Sun, Y.; Watkins, B. & Ketterson, J. B. (2006). Bound excitons in Cu_2O: Efficient internal free exciton detector, *Phys. Rev. B* 74, 235204.

Jang, J. I. & Ketterson, J. B. (2007). Impact of impurities on orthoexciton-polariton propagation in Cu_2O, *Phys. Rev. B* 76, 155210.

Jang, J. I. & Ketterson, J. B. (2008). Suppression of molecule formation for orthoexciton-polaritons in Cu_2O, *Solid State Commun.* 146, 128.

Jang, J. I.; Sun, Y. & Ketterson, J. B. (2008). Indirect generation of quadrupole polaritons from dark excitons in Cu_2O, *Phys. Rev. B* 77, 075201.

Jang, J. I.; Sun, Y.; Mani, S. & Ketterson, J. B. (2008). Resonantly enhanced reflection of quadrupole polaritons in Cu_2O, *Appl. Phys. Lett.* 93, 121111.

Kasprzak, J.; Richard, M.; Kundermann, S.; Baas, A.; Jeambrun, P.; Keeling, J. M. J.; Marchetti, F. M.; Szymanska, M. H.; Andre, R.; Staehli, J. L.; Savona, V.; Littlewood, P. B.; Deveaud, B. & Dang, L. S. (2006). Bose-Einstein condensation of exciton polaritons, *Nature* 443, 409.

Kavoulakis, G. M.; Chang, Y. -C. & Baym, G. (1997). Fine structure of excitons in Cu_2O, *Phys. Rev. B* 55, 7593.

Kuwabara, G.; Tanaka, M. & Fukutani, H. (1977). Optical absorption due to paraexciton of Cu_2O, *Solid State Commun.* 21, 599.

Kuwata-Gonokami, M.; Shimano, R. & Mysyrowicz, A. (2002). Phase-coherent manipulation of cold biexcitonic waves, *J. Phys. Soc. Jpn.* 71, 1257.

Lagoudakis, K. G.; Wouters, M.; Richard, M.; Baas, A.; Carusotto, I.; Andre, R.; Dang, L. S. & Deveaud-Pledran, B. (2008). Quantized vortices in an exciton-polariton condensate, *Nat. Phys.* 4, 706.

Lai, C. W.; Kim, N. Y.; Utsunomiya, S.; Roumpos, G.; Deng, H.; Fraser, M. D.; Byrnes, T.; Recher, P.; Kumada, N.; Fujisawa, T. & Yamamoto, Y. (2007). Coherent zero-state and π-state in an exciton-polariton condensate array, *Nature* 450, 529.

Landau, L. D. & Lifshitz, E. M. (1977). *Quantum Mechanics*, 3rd ed. Pergamon, New York. pp. 339.

Langer, V.; Stolz, H. & von der Osten, W. (1995). Picosecond quantum-beat spectroscopy of quadrupole polaritons in Cu_2O, *Phys. Rev. B* 51, 2103.

Lin, J. L. & Wolfe, J. P. (1993). Bose-Einstein condensation of paraexcitons in stressed Cu_2O, *Phys. Rev. Lett.* 71, 1222.

Liu, Y. & Snoke, D. (2005). Resonant two-photon excitation of 1s paraexcitons in cuprous oxide, *Solid State Commun.* 134, 159.

Mani, S.; Jang, J. I.; Ketteron, J. B. & Park, H. Y. (2009). High-quality Cu_2O crystals with various morphologies grown by thermal oxidation, *J. Cryst. Growth* 311, 3549.

Mani, S.; Jang, J. I. & Ketterson, J. B. (2009). Large third-order susceptibility and third-harmonic generation in centrosymmetric Cu_2O crystal, *Opt. Lett.* 34, 2817.

Mani, S.; Jang, J. I. & Ketterson, J. B. (2010). Nonlinear optical processes at quadrupole polariton resonance in Cu_2O as probed by a Z-scan technique, *Phys. Rev. B* 82, 113203.

Markworth, P. R.; Chang, R. P. H.; Sun, Y.; Wong, G. K. L. & Ketterson, J. B. (2001). Epitaxial stabilization of orthorhombic cuprous oxide films on MgO (110), *J. Mater. Res.* 16, 914.

Mysyrowicz, A.; Trauernicht, D. P.; Wolfe, J. P. & Trebin, H. -R. (1983). Stress dependence of the paraexciton in Cu_2O, *Phys. Rev. B* 27, 2562.

Naka, N. & Nagasawa, N. (2002). Nonlinear paraexciton kinetics in a potential trap in Cu_2O under two-photon resonance excitation, *Phys. Rev. B* 65, 245203.

O'Hara, K. E.; Suilleabhain, L. O. & Wolfe, J. P. (1999). Strong nonradiative recombination of excitons in Cu_2O and its impact on Bose-Einstein statistics, *Phys. Rev. B* 60, 10565.

O'Hara, K. E.; Gullingsrud, J. R. & Wolfe, J. P. (1999). Auger decay of excitons in Cu_2O, *Phys. Rev. B* 60, 10872.

O'Hara, K. E. & Wolfe, J. P. (2000). Relaxation kinetics of excitons in Cu_2O, *Phys. Rev. B* 62, 12909.

Olsen, L. C.; Addis, F. W. & Miller, W. (1982). Experimental and theoretical studies of Cu_2O solar cells, *Solar Cells* 7, 247.

Pekar, S. I.; Piskovoi, V. N. & Tsekvava, B. E. (1981). Transmission and reflection of light at the vacuum-crystal interface in the region of a quadrupole exciton transition, *Sov. Phys. Solid State* 23, 1113.

Pestov, D.; Wang, X.; Ariunbold, G. O.; Murawski, R. K.; Sautenkov, V. A.; Dogariu, A/; Sokolov, A. V. & Scully, M. O. (2008). Single-shot detection of bacterial endospores via coherent Raman spectroscopy, *Proc. Natl. Acad. Sci. U.S.A.* 105, 422.

Petroff, Y. P.; Yu, P. Y. & Shen, Y. R. (1975). Study of photoluminescence in Cu_2O, *Phys. Rev. B* 12, 2488.

Pushkarsky, M. B.; Webber, M. E.; Macdonald, T. & Patel, C. K. N. (2006). Sub-parts-per-billion level detection of NO_2 using room-temperature quantum cascade lasers, *Proc. Natl. Acad. Sci. U.S.A.* 103, 10846.

Schmidt-Whitley, R. D.; Martinez-Clemente, M. & Revcolevschi, A. (1974). Growth and microstructural control of single crystal cuprous oxide Cu_2O, *J. Cryst. Growth* 23, 113.

Serebryakov, V. A.; Boiko, E. V.; Petrishchev, N. N. & Yan, A. V. (2010). Medical applications of mid-IR lasers. Problems and prospects, *J. Opt. Technol.* 77, 6.

Sheik-Bahae, M.; Said, A. A.; Wei, T.; Hagan, D. J. & Van Stryland, E. W. (1990). Sensitive measurement of optical nonlinearities using a single beam, *IEEE J. Quantum Electron.* 26, 760.

Sheik-Bahae, M.; Hutchings, D. C. ; Hagan, D. J. & Van. Stryland, E. W. (1991). Dispersion of bound electronic nonlinear refraction in solids, *IEEE J. Quantum Electron.* 27, 1296.

Snoke, D. W.; Wolfe, J. P. & Mysyrowicz, A. (1987). Quantum saturation of a bose gas; excitons in Cu_2O, *Phys. Rev. Lett.* 59, 827.

Snoke, D. W.; Wolfe, J. P. & Mysyrowicz, A. (1990). Evidence for Bose-Einstein condensation of excitons in Cu_2O, *Phys. Rev. B* 41, 11171.

Snoke, D. W. & Negoita, V. (2000). Pushing the Auger limit: Kinetics of excitons in traps in Cu_2O, *Phys. Rev. B* 61, 2904.

Sun, Y.; Wong, G. K. L. & Ketterson, J. B. (2001). Production of 1s quadrupole-orthoexciton polaritons in Cu_2O by two-photon pumping, *Phys. Rev. B* 63, 125323.

Takagahara, T. (1985). Theory of dephasing relaxation of excitonic polaritons, *Phys. Rev. B* 31, 8171.

Tayagaki, T.; Mysyrowicz, A. & Kuwata-Gonokami, M. (2006). Collision between supercooled excitons in Cu_2O studied by time-resolved Lyman spectroscopy, *Phys. Rev. B* 74, 245127.

Toth, R. S.; Kilson, R. & Trivich, D. (1960). Preparation of large area single-crystal cuprous oxide, *J. Appl. Phys.* 31, 1117.

Trauernicht, D. P. & Wolfe, J. P. (1986). Drift and diffusion of paraexcitons in Cu_2O: Deformation-potential scattering in the low-temperature regime, *Phys. Rev. B* 33, 8506.

Trebin, H. -R.; Cummins, H. Z. & Birman, J. L. (1981). Excitons in cuprous oxide under uniaxial stress, *Phys. Rev. B* 23, 597.

Utsunomiya, S.; Tian, L.; Roumpos, G.; Lai, C. W.; Kumada, N.; Fujisawa, T.; Kuwata-Gonokami, M.; Loffler, A.; Hofling, S.; Forchel, A. & Yamamoto, Y. (2008). Observation of Bogoliubov excitations in exciton-polariton condensates, *Nat. Phys.* 4, 700.

Vollmer, F. & Arnold, S. (2008). Whispering-gallery-mode biosensing: label-free detection down to single molecules, *Nature* 5, 591.

Waters, R. G.; Pollak, F. H.; Bruce, R. H. & Cummins, H. Z. (1980). Effects of uniaxial stress on excitons in Cu_2O, *Phys. Rev. B* 21, 1665.

Wolfe, J. P.; Lin, J. L. & Snoke, D. W. (1995). Bose-Einstein condensation of a nearly ideal gas: Excitons in Cu_2O, In: *Bose-Einstein Condensation*, Griffin, A.; Snoke, D. W. & Stringari, S. (Ed.), Cambridge University Press, Cambridge, England. pp. 281-329.

Wolfe, J. P. & Jang, J. I. (2005). New perspectives on kinetics of excitons in Cu_2O, *Solid State Commun.* 134, 143.

Yoshioka, K. & Kuwata-Gonokami, M. (2006). Dark excitons in Cu_2O crystals for two-photon coherence storage in semiconductors, *Phys. Rev. B* 73, 081202(R).

Yu, P. Y. & Shen, Y. R. (1975). Resonance Raman studies in Cu_2O. I. The phonon-assisted 1*s* yellow excitonic absorption edge, *Phys. Rev. B* 12, 1377.

Zipfel, W. R.; Williams, R. M. & Webb, W. W. (2003). Nonlinear magic: Multiphoton microscopy in the biosciences, *Nat. Biotechnol.* 21, 1369.

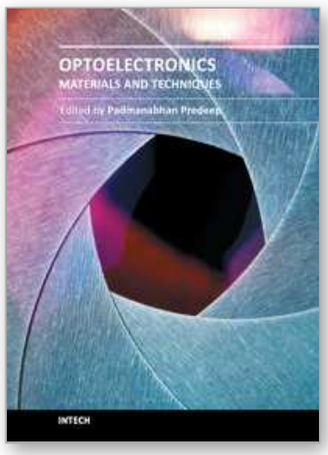

Optoelectronics - Materials and Techniques
Edited by Prof. P. Predeep

ISBN 978-953-307-276-0
Hard cover, 484 pages
Publisher InTech
Published online 26, September, 2011
Published in print edition September, 2011

Optoelectronics - Materials and Techniques is the first part of an edited anthology on the multifaceted areas of optoelectronics by a selected group of authors including promising novices to the experts in the field. Photonics and optoelectronics are making an impact multiple times the semiconductor revolution made on the quality of our life. In telecommunication, entertainment devices, computational techniques, clean energy harvesting, medical instrumentation, materials and device characterization and scores of other areas of R&D the science of optics and electronics get coupled by fine technology advances to make incredibly large strides. The technology of light has advanced to a stage where disciplines sans boundaries are finding it indispensable. Smart materials and devices are fast emerging and being tested and applications developed in an unimaginable pace and speed. Here has been made an attempt to capture some of the materials and techniques and underlying physical and technical phenomena that make such developments possible through some real time players in the field contributing their work and this is sure to make this collection of essays extremely useful to students and other stake holders such as researchers and materials scientists in the area of optoelectronics.

How to reference
In order to correctly reference this scholarly work, feel free to copy and paste the following:

Joon I. Jang (2011). Cuprous Oxide (Cu2O): A Unique System Hosting Various Excitonic Matter and Exhibiting Large Third-Order Nonlinear Optical Responses, Optoelectronics - Materials and Techniques, Prof. P. Predeep (Ed.), ISBN: 978-953-307-276-0, InTech, Available from: http://www.intechopen.com/books/optoelectronics-materials-and-techniques/cuprous-oxide-cu2o-a-unique-system-hosting-various-excitonic-matter-and-exhibiting-large-third-order

INTECH
open science | open minds

InTech Europe
University Campus STeP Ri
Slavka Krautzeka 83/A
51000 Rijeka, Croatia
Phone: +385 (51) 770 447
Fax: +385 (51) 686 166
www.intechopen.com

InTech China
Unit 405, Office Block, Hotel Equatorial Shanghai
No.65, Yan An Road (West), Shanghai, 200040, China
中国上海市延安西路65号上海国际贵都大饭店办公楼405单元
Phone: +86-21-62489820
Fax: +86-21-62489821

IntechOpen